CANADIAN THESES ON MICROFICHE

I.S.B.N.

THESES CANADIENNES SUR MICROFICHE

National Library of Canada
Collections Development Branch

Canadian Theses on
Microfiche Service

Ottawa, Canada
K1A 0N4

Bibliothèque nationale du Canada
Direction du développement des collections

Service des thèses canadiennes
sur microfiche

NOTICE

The quality of this microfiche is heavily dependent upon the quality of the original thesis submitted for microfilming. Every effort has been made to ensure the highest quality of reproduction possible.

If pages are missing, contact the university which granted the degree.

Some pages may have indistinct print especially if the original pages were typed with a poor typewriter ribbon or if the university sent us a poor photocopy.

Previously copyrighted materials (journal articles, published tests, etc.) are not filmed.

Reproduction in full or in part of this film is governed by the Canadian Copyright Act, R.S.C. 1970, c. C-30. Please read the authorization forms which accompany this thesis.

THIS DISSERTATION
HAS BEEN MICROFILMED
EXACTLY AS RECEIVED

AVIS

La qualité de cette microfiche dépend grandement de la qualité de la thèse soumise au microfilmage. Nous avons tout fait pour assurer une qualité supérieure de reproduction.

S'il manque des pages, veuillez communiquer avec l'université qui a conféré le grade.

La qualité d'impression de certaines pages peut laisser à désirer, surtout si les pages originales ont été dactylographiées à l'aide d'un ruban usé ou si l'université nous a fait parvenir une photocopie de mauvaise qualité.

Les documents qui font déjà l'objet d'un droit d'auteur (articles de revue, examens publiés, etc.) ne sont pas microfilmés.

La reproduction, même partielle, de ce microfilm est soumise à la Loi canadienne sur le droit d'auteur, SRC 1970, c. C-30. Veuillez prendre connaissance des formules d'autorisation qui accompagnent cette thèse.

LA THÈSE A ÉTÉ
MICROFILMÉE TELLE QUE
NOUS L'AVONS REÇUE

NL-339 (r. 82/08)

Canada

UNIVERSITÉ D'OTTAWA
UNIVERSITY OF OTTAWA

COMPUTER-BASED SYSTEM FOR ACQUISITION OF DOSIMETRIC DATA

by

Yuk Sum Tam

A thesis
presented to the School of Graduate Studies and Research
of the University of Ottawa
in partial fulfillment of the
requirements for the degree of
M.A.Sc. (Electrical Engineering)

Ottawa, Ontario, 1983

University of Ottawa requires the signatures of all persons using or photocopying this thesis. Please sign below, and give address and date.

ABSTRACT

To assess potential health hazards due to electromagnetic radiation, quantitative methods which would allow one to determine the dose rate resulting from specific exposure conditions, are needed. Using a miniature electric probe for determining electric field in biological media for a given exposure condition is one of techniques which allows us to measure the intensity of electric field directly. However this technique is time-consuming. If a computer system is employed, a large saving in time and manpower can be achieved.

The objective of this project is to develop a computer controlled scanning system for measurement of the distribution of the specific absorption rate in simulated biological bodies irradiated by selected sources in both far and near field. This thesis deals with the electronic design and development of computer programming as related to a computer-based system for acquisition of dosimetric data. The testing methods and experimental results for the scanning system and the electronic network are presented to demonstrate that the system meets the basic requirement. Finally, suggustions for further development are discussed.

ACKNOWLEDGEMENTS

The author wishes to express his sincere gratitude to his supervisor, professor S.S. Stuchly, for his guidance throughout the course of this research.

Thanks are also due to other staff members involved in the project, M.A. Stuchly, A. Kraszewski, M. Barski and G. Hartsgrove. Thanks are also due to other members of the Department of Electrical Engineering, especially Mohammed Master, Benito Carraro and Steve Symons for their invaluable assistance in the execution of this project. The financial support for this research by the National Sciences and Engineering research Council of Canada, the Ontario Ministry of Labour, the office of Naval Research and Health and Welfare Canada is greatly appreciated.

LIST OF SYMBOLS

AC	Alternate current
A/D	Analog to digital converter
B_m	An empirical constant
B.P.F.	Bandpass filter
c	Specific heat of the phantom material in J/kg °C
DC	Direct current
E_T	Total electric field intensity in V/m
I/O	Input / output
P_c	Power absorbed in the empty chamber in W
P_{PH+C}	Power absorbed in the chamber and phantoms in W
P_T	Total transmited power in W
RF	Radio frequency
RFI	Radio frequency interference
R.M.S.	Root mean square
SAR	Specific Absorption Rate in W/kg
V_T	Total output voltage of the probe
W	Power absorbed in the phantom model in W
w(m)	mass of the model in kg.
σ	Electrical conductivity of the medium in S/m
ρ	Density of the medium kg/m^3

ΔT	Temperature rise in the phantom model in °C
Δt	Elapsed time of the experiment in s.

CONTENTS

LIST OF TABLES

LIST OF FIGURES

Chapter I

INTRODUCTION

The increasing use of radiowaves and microwaves in communication systems, new medical devices, industrical and domestic applications for heating purposes has resulted in exposure of the the human population to appreciable levels of electromagnetic radiation. Certain sectors of the population and certain occupational groups are continuously exposed to significant exposure. Examples include people living in the immediate vicinity of commercial broadcast stations, satellite communication stations and powerful military radio installations. Another example of potential exposure of the general population in the domestic is microwave oven used for cooking. Other exposures are essentially occupational. These include workers using radiowave sealing devices, workers using microwave ovens for heating purpose in restaurants and factories, personnel in the immediate vicinity of radar installations, employees of broadcasting stations and some teamsters and police officers who are heavy users of CB and mobile radios. Health hazards of electromagnetic radiation have been reported on many occasions [1]. Growing concern about possible health hazards produced by electromagnetic radiation leads to an increased intensity of research.

1.1 THE PROBLEM

Most researchers accept the fact that high level power density of electromagnetic radiation can result in thermal effects. They argue that the harmful effects of radiation are due exclusively to the heating of tissues. On the other hand, low-level radiation cannot be overlooked. Low-level radiation which is too weak to cause gross heating of tissues, can affect neural and immunologic function in animals and man [1] - [3]. Most of these reports have come from the USSR and other Eastern European countries. Due to limited knowledge and differing opinions about the biological effects of electromagnetic radiation, various exposure standards are used worldwide at the present time. In the United States, the exposure standard for continuous exposure has been lowered to 1 mw/cm^2 from 10 mw/cm^2 [1]. In contrast, the exposure standard in China is 50 $\mu w/cm^2$ [1]. The Soviet Union has set their safety standard a hundred times lower than those in the United States. Their maximum allowable power density is 10 $\mu w/cm^2$ [1].

Several countries, including Sweden, are in the process of revising their safety standards downward from the previously accepted levels of 10 mw/cm^2 [4].

1.1.1 Motivation

Because of the expanding usage of electromagnetic radiation and disagreement over safe exposure levels, a new concept and understanding of the biological effects of electromagnetic radiation is necessary. Such knowledge is useful for evaluating and setting up reliable radiation safety standards to protect the general public as well as occupational personnel from adverse effects of radiation. It is also necessary to define hazard levels and understand physical effects. Such knowledge gained by studying the interaction of organisms and electromagnetic radiation may also be useful in developing electromagnetic techniques for medial diagnosis [5] and cancer therapy [6]. It is evident that quantitative methods which would allow one to determine the dose rate resulting from specific exposure conditions, are needed.

The purpose of this project is to develop a computer controlled scanning system for the measurement of the distribution of the specific absorption rate (SAR) in simulated biological bodies irradiated by selected sources in both far and near-fields. This project involves mechanics, electronics, radiowave and microwave techniques and computer programming. A group of six persons are presently involved in this project. The areas in which I participated in this project were electronic design and computer programming.

1.1.2 Outline

This thesis deals with electronic design and development of computer programming as related to a computer-based system for acquisition of dosimetric data. In the first chapter, background knowledge and parameters that affect whole-body energy absorption are discussed. The works which have previously been done in determining the dose rate, are reviewed. At the end of this chapter, a general description of the computer-based scanning system is presented. In the second chapter, a block diagram of the system is introduced. The hardware implementation and functions of each individual component are described in detail. The software development is also presented. In the third chapter, the testing methods and experimental results for the scanning system and the electronic network are presented and discussed. Finally, chapter four gives a general discussion of the results and presents the conclusion.

1.2 BACKGROUND REVIEW

The amount of energy absorbed by humans and animals is an essential element in the study of possible biological effects. A parameter called the Specific Absorption Rate (SAR) has been adopted worldwide at the present time for describing the dose rate due to exposure to electromagnetic fields. The specific absorption rate is defined as the time

rate at which energy is absorbed by the absorbing body, normalized to the mass of the body.

$$SAR = \left(\frac{\sigma}{\rho}\right) E_T^2 \quad [W kg^{-1}] \qquad (1)$$

where E_T is the total electric field intensity in V/m, σ is the effective electrical conductivity of the medium in S/m, ρ is the density of the medium in kg/m^3.

Unlike ionizing radiation which travels along straight lines within the body, electromagnetic radiation experiences reflection, refraction and diffraction effects within the biological body due to the varying dielectric and absorption properties of the body. The whole-body electromagnetic energy absorption is strongly dependent on several parameters of the exposure field [4] such as:

(i) Frequency of the exposure field.

(ii) Intensity of the exposure field.

(iii) Polarization of the exposure field.

as well as parameters of the body, such as:

(i) Size and shape of the biological body.

(ii) Dielectric properties of the biological body.

Furthermore, the source-object configuration is also important. The exposure may either be in the far-field or in the near-field. The physical environment, such as the presence of conducting ground or reflecting surfaces, may also significantly affect electromagnetic energy absorption of biological bodies.

In general, biological bodies are complex from the viewpoint of electromagnetic wave theory as they are irregular in shape and have non-homogeneous dielectric properties. Therefore, different quantitative techniques are required in order to obtain the absorbed dose rate of the biological bodies due to electromagnetic radiation. Generally speaking, two major techniques are employed. They are theoretical dosimetry and experimental dosimetry.

1.2.1 Theoretical Dosimetry

In theoretical dosimetry, most of the analysis is based on a plane-wave approximation which is valid only in the far-field region. The general procedure is to calculate the absorbed energy in biological bodies by solving Maxwell's equations. However, because of complexity of the equations and the complexity of boundary conditions, different techniques to solve equations have been employed. These include a long wavelength approximation, numerical techniques, analytical cylindrical models and geometrical

optics techniques [7]. Each technique is useful and provides information in a certain range of frequencies.

By applying different techniques, several simplified models of humans and animals or their parts exposed in the far-field have been analyzed. These include three plane layers of tissue, homogeneous spherical models, ellipsoidal models, cylindrical models and block models of man composed of cubical cells [7].

Theoretical dosimetry in the far-field has been investigated for a long time. However most occupational exposure is in the near-field, for example, workers using plastic welding machines for sealing or joining sheets of plastic materials. As a result, researchers give more attention to the near-field exposure. Near-field analysis has been pursued, but the calculations for the near-field case are more difficult than those for the far-field case. So far, only simple sources have been analyzed [7]. These include short dipoles and small loops.

1.2.2 Experimental Dosimetry

For complex models and source configurations, theoretical calculations are very difficult [10]. An alternate approach to quantify hazardous fields is to perform measurements inside phantom models which simulate the electrical properties, size and shape of biological

bodies. This method has been developing in parallel with theoretical dosimetry for specific applications to:

(i) Verify the theoretical results or predictions,

(ii) Determine the total SAR in experimental animals,

(iii) Determine the total SAR or distribution in models whose size and shape are close to real biological bodies, and

(iv) Determine the SAR in models and animals in the near-field exposure where theoretical analysis is prohibitively difficult.

Models and living animals are frequently used in experimental dosimetry. However, phantom models which have the same complex permittivity as human tissue, are preferred [8]. It is because models can be made to accurately simulate the human body well in both geometry and size. Either full size models or scaled models are used. For near-field or part-body exposure, full size models are preferred. For whole body exposure situations, reduced scale models are preferred because they are easy to handle and require less working space. From electromagnetic field theory, a body reduced by a scale factor S in all dimensions may be used to obtain the absorption characteristic of a full size body, provided that the [9]:

(i) Dielectric constant of the scaled model is

the same as the full size model.

(ii) Electrical conductivity of the scaled model is S times.

(iii) Irradiation frequency is scaled up by the factor S.

With this scaling the power absorption pattern for the scaled model is the same as those for a full size model, with the exception that the magnitude of the absorption is increased by a factor S for a given field intensity. This allows a great reduction in applied power when a reduced size model is used. The following techniques have been used in experimental dosimetry.

I. Infrared Thermographic Method

The thermographic method has been developed by Guy [10]-[13]. It has proved to be a very useful and fast tool to study scaled down phantom models exposed to electromagnetic fields. In this technique, a prepared phantom model is first exposed to high intensity radiation. A high-power source is used in order to heat up the model in the shortest possible time. If the exposure time is long, errors result due to thermal diffusion smearing the distribution. After a short exposure, the model is rapidly disassembled. The temperature pattern over the surface of separation is observed and recorded by means of a thermographic camera. The SAR can be calculated from

$$SAR = \frac{C\Delta T}{\Delta t} \qquad (2)$$

where C is the specific heat capacity of the phantom material in J/kg °C, ΔT is the temperature rise in the phantom model in °C, Δt is the elapsed time of the experiment in seconds.

Thermographic techniques have proved successful for obtaining dosimetric information on scaled models exposed to electromagnetic fields. The errors occuring in this technique arise mainly due to thermal diffusion and the imperfections of the thermographic camera. Thermal diffusion usually occurs in the region of highest temperature gradient on the surface of separation.

II. Power Measurement Technique

The power measurement technique [14] is a simple method to determine the total amount of energy absorbed by phantom models or living animals during radiation exposure. A block diagram of the power measurement method is shown in Fig. 1. A differential power meter system is used to measure the incident and reflected powers and the power delivered to a matched load. First, the power, P_C, absorbed in the exposure chamber with an empty phantom in place is measured by the differential power meter. Then, the phantom is filled and placed in the chamber and the power, P_{PH+C}, absorbed by this configuration is measured again. The amount of power, W, absorbed by the phantom can be calculated,

$$W = P_{PH+C} - P_C \qquad (3)$$

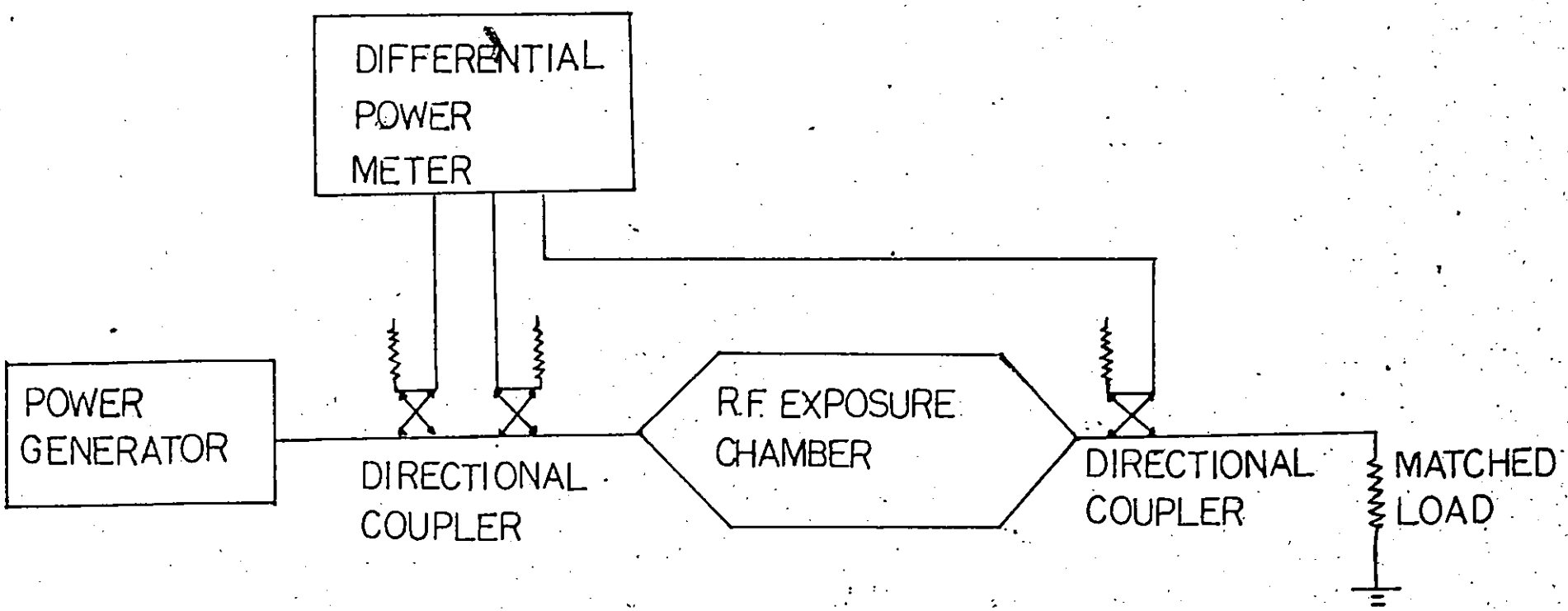

Figure 1: Block diagram of power measurement method

By using this method, only the total SAR can be measured.

III. Calorimetric Method

The calorimetric method [15] is used to determine the total power absorbed by phantom models. A prepared phantom model is placed in a low dielectric insulated container and is irradiated by a high intensity source. After a short period of time, the temperature of the model is measured. By assuming the absence of thermal radiation and convection, the power being absorbed by the model is given by

$$W = \frac{C w \Delta T}{\Delta t} \qquad (4)$$

where W is the net power absorbed by the model in watts, w is the mass of the model in kg, C is the specific heat capacity of the model in J/kg $^{\circ}$C, ΔT is the temperature increase of the model in $^{\circ}$C, Δt is the elapsed time of the experiment in seconds. Again, only the total SAR can be determined by using this technique.

IV. Thermometric Probe Technique

In the thermometer probe technique [16] [17] the temperature increment due to radiation exposure is measured by a digital thermometer with a thermoelectric probe. Small holes are drilled in a phantom model to insert the probe

before and after irradiation. Before irradiation, the temperature of the model is recorded. Then the model is exposed to a high intensity radiation for a short time. At the end of exposure, the probe is inserted again. The increase in temperature is recorded. Finally, a graph of temperature profile vs probe position is obtained. The intensity of the electric field and the SAR can be determined for a given mass, density and specific heat capacity of the model.

V. Electric Probe Method

The basic idea of the electric probe technique [18]-[22] is similiar to that of the thermometric probe technique. Instead of thermoelectric probes, small electric field probes are used. The probe is very small that it does not affect or perturb the field. The intensity of the electric field in biological media for a given exposure condition is measured directly. Several small holes are drilled in a prepared phantom model for insertion of the probe. The model is then placed in an anechoic chamber and is irradiated using a medium power source. The distribution of the electric field intensity can be measured and the SAR can be calculated for a given model.

VI. Comparison of the Methods and Techniques of Experimental Dosimetry

Since the electromagnetic energy absorption is strongly dependent on several parameters of the biological body, the SAR distribution gives more information about potential biological hazards than the total SAR does. Therefore, techniques which can determine SAR distribution, are preferred. Among those experimental dosimetric techniques mentioned above, only thermography, thermometric probe and implantable electric field probe techniques allow one to determine the SAR distribution. A comparison of these dosimetric techniques is shown in table 1. It is evident that the implantable probe technique has advantages over other techniques. It allows real-time measurements to be performed in phantom models or specimens during exposure to a medium power radiation source. If a triaxial probe is used, the three orthogonal components of the electric field vector can be measured [20] since the electromagnetic energy absorption may, for some anisotropic media, be dependent upon the orientation of the electric field. This technique is suitable for both near-field and far-field measurements.

Table 1. Comparsicn of dcsimetric techniques.

	E-field Prcbe	Thermometer Probe	Thermography
Measured parameter	Electric-field intensity	Temperature	Temperature
Dosimetric approach	Direct electric-field measurement	Direct temperature measurement after exposure	Direct temperature measurement after exposure
Parameter used to calculate SAR	Conductivity and density of the phantom model	Mass, density and specific heat of phantom model	Mass, density specific heat of phantom model and infrared emittance
Sensitivity to external field	< 10 mw/cm^2 [18]	>10 mw/cm^2 [18]	>100 mw/cm^2 [18]
Source intensity	Medium	High	Very high
S A R sensitivity (1 s exposure)	0.05 W/Kg at 2450 Mbz in muscle-equivalent medium [18]	0.2 W/Kg in muscle-equivalent medium [18]	0.7 W/kg in muscle-equivalent medium [18]
Phantom model	Full size or model	Full size or scaled model	Scaled model only (power level limitation)
Real time measurement	Yes	No	No
Suitable for in vivo	Yes	Yes	No
Measurement capability	Single point or line scan	Single point or line measurement	Rapid planar scan

Because of the thermal properties and regulatory mechanisms of biclogical bodies, it is hard to simulate the thermal characteristics of the bodies, such as: the cooling effect cf the blood system. It is more logical to base dosimetric measurements on the internal electric field measurement and relate the results to potential biological hazards [8]. Among those experimental dosimetric techniques, only the last technique allows us to measure the electric field directly. Therefore the electric-field probe technique is preferred.

1.3 PROPOSED METHOD

In order to measure the distribution of the electric field inside biclogical bodies, an electric-field probe technique is used. The major limitation cf this technique is that it is time-consuming. For a given biological body, a large number of measurements have to be performed within the body in order tc obtain the distribution of the electric field or SAR. If a computer-controlled scanning system can be used, a large saving in time and manpower can be achieved. Furthermore, the quality can be improved by elimination of human error. The data can be stored in the computer memory for display and storage or for further analysis. Also, the use of a computer for scanning control and data acquisition offers frequent reiteratien of the system and allows one to introduce corrections for the

amplitude distribution of the antenna or other radiator used in the experiment.

1.3.1 Principle of operation

A block diagram of a proposed computer-controlled scanning system is shown in Fig. 2 . It consists of a power generator, a phantom model, an electric field probe with a detector, a computer with a display unit and a scanning control system. In the initial mode, the positions of the holes in the phantom model are identified and stored in the computer. The computer directs the scanning control system to move the probe to a particular preselected position in the model identified in the initial procedure. After the probe is lowered into the hole, the intensity of the electric field at that specific location is measured and stored in the computer. The probe is then moved to another hole where the procedure is repeated until all holes are scanned. Finally, the acquired data are displayed by the display unit.

1.3.2 Specifications of the computer-controlled scanning system

The system should perform according to the following specification

(i) Scanning volume should be about $180 \times 50 \times 30$ cm^3.

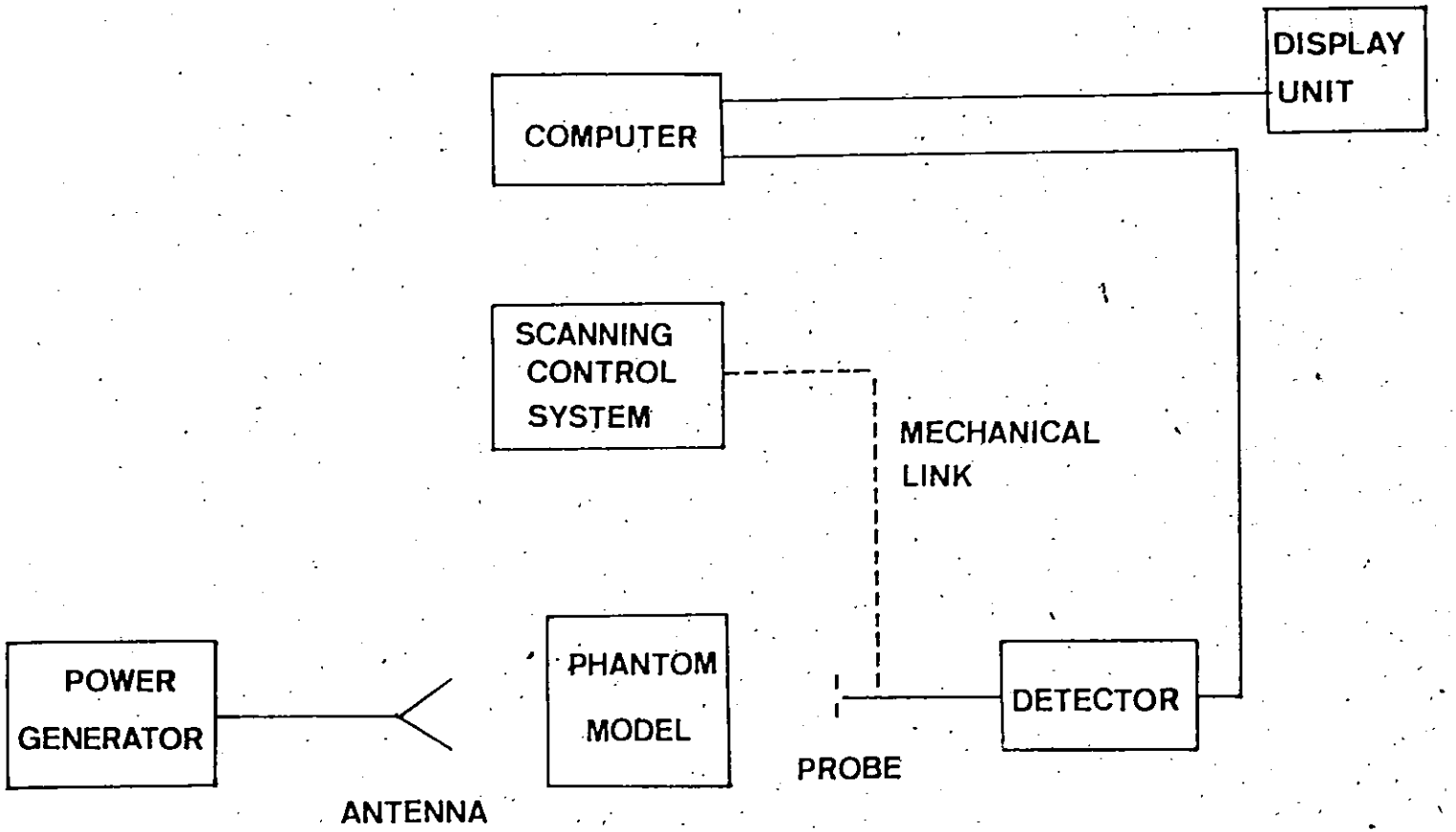

Figure 2: Simplified block diagram of computer-controlled scanning system

(ii) Repeatability of probe positioning in a particular location should be better than ± 0.5mm.

(iii) the output signal from the probe and associated signal processing units should normally be proportional to the square of the electric field intensity (power) at a specific location.

(iv) Data should be stored in the memory to be used for visual inspection in the form of a print-out or recorded by a X-Y plotter.

Chapter II

SYSTEM DESCRIPTION

In this chapter, hardware implementation and software develcpment are discussed. In the first section, the implementation of each block shown in Fig. 2 is discussed. The description of individual components and special design units are also presented. In the last section, the general concept of software and implementation are described.

2.1 HARDWARE IMPLEMENTATION

2.1.1 Block Diagram Implementation

I. Electric Field Probe

Two different tri-axial electric field probes shown in Fig. 3 which are similiar to the one described in [18]-[22], are used in this project to measure the intensity of the electric field within simulated biological bodies. These are the NARDA model BRH 14 and the EIT model 979. The probes are very small and cause minimal field perturbation. They are developed recently by BRH (Bureau of Radiological Health) in co-operation with NARDA and EIT (Electronic Instrumentation and Technology), respectively. The first

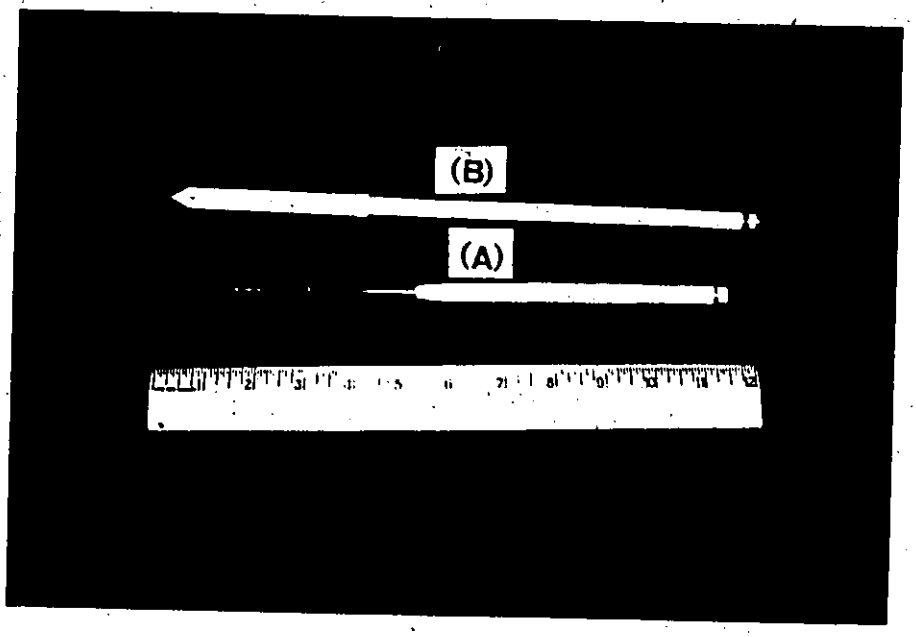

Figure 3: Two triaxial probes (a) NARDA model BPH 14, (b) EIT model 979

one is used at frequencies above 300 MHz and the second one is used at lower frequencies below 300 MHz. Each probe consists of three orthogonal miniature dipoles shunted by Schottky-barrier diodes. The output of each diode is fed to the output connector by a pair of high-impedance leads to minimize perturbation of the measured field. The radio-frequency signal from the power source, is converted by the diode to a DC signal or an audio-frequency signal if amplitude modulation of the power source is used.

The probes utilize Schottky diodes and therefore, the noise characteristic of the diode must be well understood. In general, Schottky diodes generate low frequency flicker noise and thermal noise [23]. Thermal noise which is caused by the random motion of electrons or charges in a conductor, is proportional to the video resistance of the diode. The flicker noise is inversly proportional to the video frequency. At low video frequencies, the flicker noise is predominant. For this reason, amplitude modulation of the radio-frequency source is employed.

II. Data Acqusition System

Noise may be induced in the probe from a number of other sources, such as man-made noise, atmospheric noise etc. At the output of the probe, the detected signal may be obscured by these noises. In order to retrieve the detected signal from the noise, a system with low-noise and a narrow-equivalent-noise bandwidth is necessary to improve the signal-to-noise ratio. A system employing a low-noise pre-amplifier and a narrow bandwidth bandpass filter is one possible solution. The components are inexpensive and the system is easy to implement. A high input impedance of the pre-amplifier is necessary to prevent loading of the probe. The bandpass filter is used to limit the noise bandwidth of the system.

Since a tri-axial probe is used, it is more economical to use a multiplexer instead of building three identical systems. A low-noise multiplexer with good isolation and minimal crosstalk is necessary. The major disadvantage is that only one of the three channels can be selected at one time.

Before the detected signal can be transfered to the computer memory, it must be converted into a digital form. The signal is first converted into a DC signal by a RMS (root mean square) to DC converter (National LH0091CD). The resulting DC signal is then digitized by an A/D converter

(Digital Equipment AD11-K). The digital data are finally stored in the memory.

III. Power Generator

An amplitude modulation system is used in order to improve the signal-tc-noise ratio. The basic amplitude mcdulation system consists of a PIN diode modulator, a RF generator, a modulating frequency generator and a RF power amplifier. The RF amplifier is used to increase the transmitted power at the output of the antenna.

The detected signal from the probe is proportional to the received power. Due to high attenuation of the phantom, the detected signal levels are very low particularily when the probe is far away from the antenna. A computer-controlled attenuator is used to control the amplitude of the signal at the input of the power amplifier. This in turn controls the power output level of the amplifier. The attenuator is used not only to widen the dynamic range of the data acquisition system, but alsc to prctect the probe from burning out when the probe is close tc the antenna.

In order to determine the power level and the frequency of the source, a small part of the signal is coupled from the main line by a directional coupler. This signal is then fed tc a power meter and a frequency meter. The result is digitized and stcred in the computer.

IV. Scanning System Control Unit

The purpose of using a scanning system control unit is to reduce the work load of the computer. It has the following functions:

(i) To inform the computer about the map of hole location,

(ii) To position the probe in a pre-selected hole after obtaining the location of the hole from the computer, and

(iii) To inform the computer about the status of the probe.

In order to position the probe in a given location within the scanning volume, three independent stepping motors are required. Each motor controls the movement of the probe along one axis only.

The probe which is rigid, can easily be broken if it should strike a hard surface. A special probe holder with safety switches are designed to protect the probe from mechanical damage. The safety switches are also connected to the control unit.

V. Computer

The computer is an essential part of the system. It is used

(i) To store the map of hole locations,

(ii) To store the values of the intensity of the electric field at various selected locations,

(iii) To control the multiplexer and the step attenuator, and

(iv) To monitor the scanning system control unit.

A computer with a large memory storage capability is necessary. In this research, a minicomputer system which consists of a Digital Equipment PDP 11/34 laboratory minicomputer and associated peripherals including A/D converter and I/C interface, is utilized.

2.1.2 Detailed Block Diagram

Finally the overall block diagram of the computer-controlled scanning system is shown in Fig. 4. To limit the reflections from the surrounding objects, experiments are performed in an anechoic chamber. The metal frame of the mechanical scanning structure is also surrounded with absorbing materials.

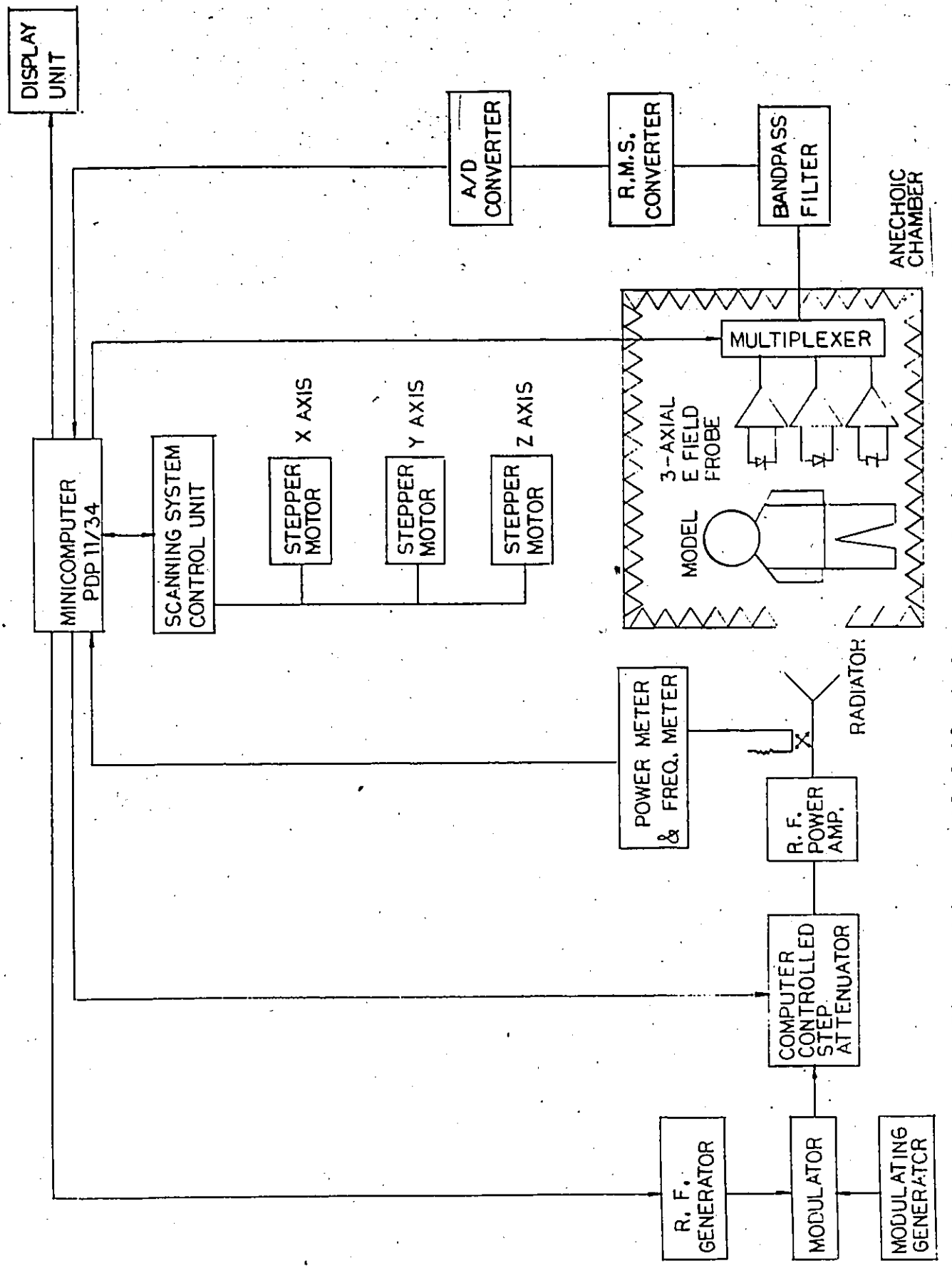

Figure 4: Detailed block diagram of the computer-controlled scanning system

2.1.3 Components Description

I. Computer

A multi-user minicomputer, PDP 11/34, running under RSX-11M is used to control and monitor all operations of the scanning system. It has three RL01K disk drives giving a total storage capacity of 15 Mbytes. This is sufficient to store the map of the hole locations and the intensity of the electric field. Its K-series laboratory peripheral modules consisting of an A/D converter and a digital I/O interface, make the interfacing and control much easier.

The computer is also used to perform signal averaging in order to improve the signal-to-noise ratio of the whole system.

II. A/D Converter

An Analog-to-Digital converter, AD 11-K, is used to sample analog data and to store the equivalent digital value for subsequent processing. The system consists of an input multiplexer, a sample-and-hold circuit and a 12-bit A/D converter. Up to 16 channels can be selected under program control. Each input channel has over-voltage protection circuity. The standard input voltage range ±5V is selected for all input channels giving a resolution of 2.44 mV. The converted value is formatted as a 12-bit right-justified offset binary number. The throughput time which is comprised

of the interchannel settling time and A/D conversion time, is 22 μsec. The A/D converter is initiated under program control.

III. Computer-controlled Attenuator

A programmable attenuator, Texscan model PA-51 (frequency range 0 - 1.3 GHz, maximum power 0.5 W), is employed to expand the dynamic range of the data acquisition system. It is equipped with a 6-bit TTL compatible control input. The attenuator can be directly controlled by the computer to provide an attenuation from 0 to 63 dB in steps of 1 dB. The switching speed is 6 ms.

IV. Digital Output Device

The DR11-K is a general purpose digital input/output interface capable of parallel transfer of up to sixteen bits of data, under program control, between a computer and external devices. Only the output lines from the DR11-K are used for control functions. Bits 15 to 10 are used to set up an attenuation value for the attenuator. Bits 9 and 8 are used to select a channel of the multiplexer.

V. Scanning System Control Unit

The scanning system control unit shown in Fig. 5, consists of a microcomputer (INTEL 8085), a memory unit, a hand-operated unit, an input and output device. The microcomputer is used as a central controller.

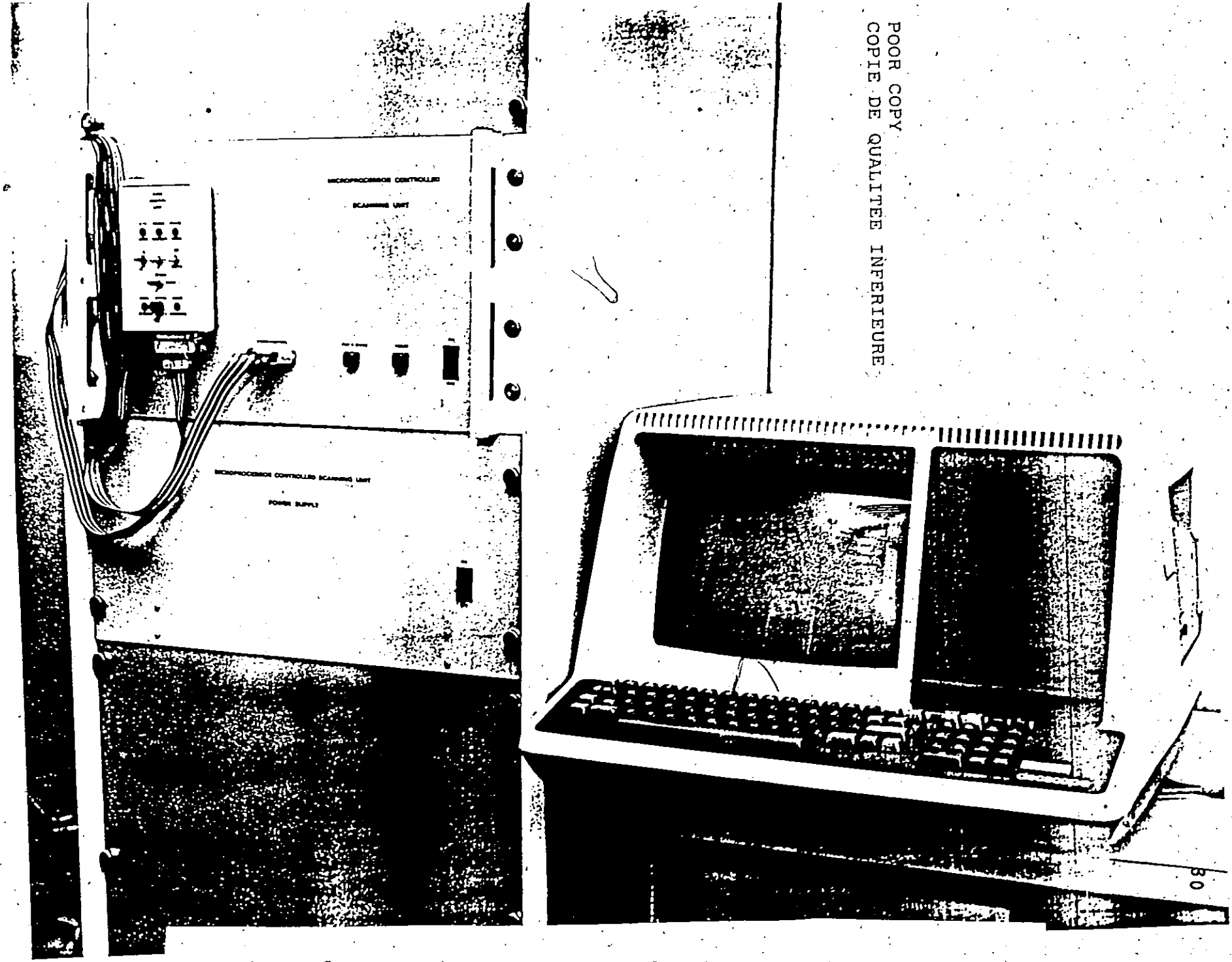

Figure 5: Scanning system control unit with a hand-operated unit

There are seven buttons on the control unit. Four of these are used to control the manual movement of the probe (manual mode). One is to select manual or remote mode. Another is to initialize the software program of the control unit and request storage of the position of the hole. The last one is a master reset button.

(i) Manual mode

In the manual mode, the position of the probe can be controlled from the hand-operated unit. For the probe directly above a selected hole, the 'store' button activates the control unit to send out the coordinates of the position to the PDP 11/34 to store it. This procedure is repeated until all selected holes are scanned. As a result, a map of the actual hole locations is stored in the computer memory.

(ii) Remote mode

In the remote mode, the computer sends out the coordinates of the hole to the control unit. The control unit positions the probe in the pre-selected hole. This procedure is repeated until all holes are scanned.

VI. Mechanical Scanning System

The mechanical parts of the scanning structure shown in Fig. 6, are made by Velmex Inc. The frame is suspended from the concrete ceiling of the laboratory. Each axis is

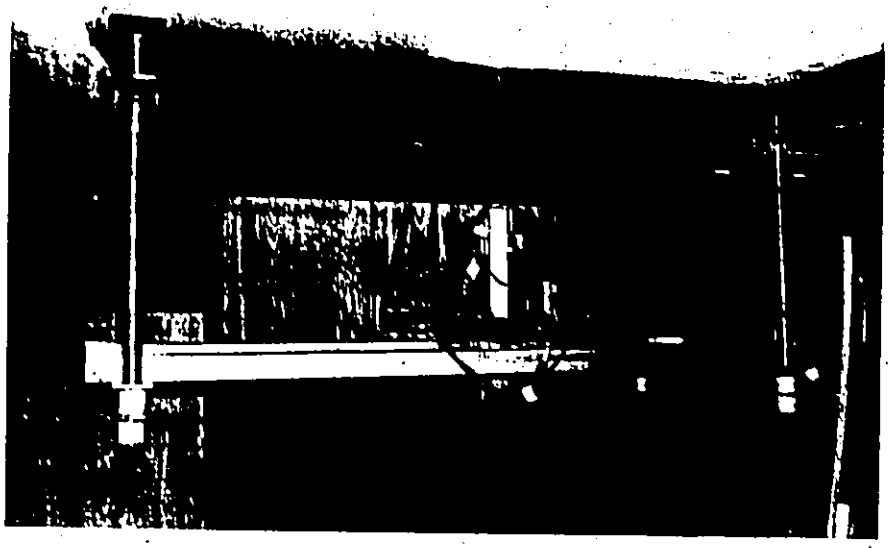

Figure 6: Mechanical scanning structure

equipped with a pair of limit (safety) switches on each end. The switches are used to prevent stepping motor from overdriving. The dimensions of the scanning structure are 2.2 m. X 0.9 m. X 0.7 m. The vertical axis ('Z-axis) is chain driven while the others are lead screw driven.

VII. Stepping Motor and Translator

Three 1.8° SIC-SYN DC stepping motors, model M092-FC09, which convert electronic signals into mechanical motion, are employed to move the probe. The motors are operated using phase-switched DC signals. Either a full-step mode or a half-step mode can be selected. Operation in the half-step mode gives finer system resolution but is slower.

Each stepping motor is actually controlled by a STM103 SLO-SYN Translator Module to simplify the electrical driving requirements. The module provides the sequencing and switching logic needed for bidirectional control of the stepping motor. After receiving pulses from the scanning system control unit, it converts the pulses into motion in the form of elementary motor steps. The speed of the stepping motor, direction and the number of steps taken can be directly controlled by the control unit. Its TTL compatible input control eliminates the interfacing problem.

Summary of movement for each axis is as follows. For the full-step mode:

Axis	Distance increments in cm/step
X	0.00127
Y	0.00127
Z	0.051

VIII. Data Acquisition System Design

The data acquisition system consists of a pre-amplifier, a multiplexer shown in Fig. 7 , a bandpass filter presented in Fig. 8 and a true RMS to DC converter depicted in Fig. 9 which are used to improve the signal-to-noise ratio. The system is battery powered.

Both the DC and modulating signal are presented at the output of the probe as the amplitude modulation system is used. However, only the modulating signal is of interest. For each data channel, a high-input-impedance and low-noise AC pre-amplifier is required to amplify the low-level modulating signal from the diode detector in the probe before it is fed to the multiplexer. The multiplexer consists of an analog switches (AD7590DI) and a decoder (CD 4555B). A minimum crosstalk ratio of -53 dB and a minimum isolation of -66 dB at 500 Hz have been achieved. Two selected inputs are required to select one of the three data channels.

An instrumentation amplifier is used to amplify the modulating signal before it is fed to a bandpass filter.

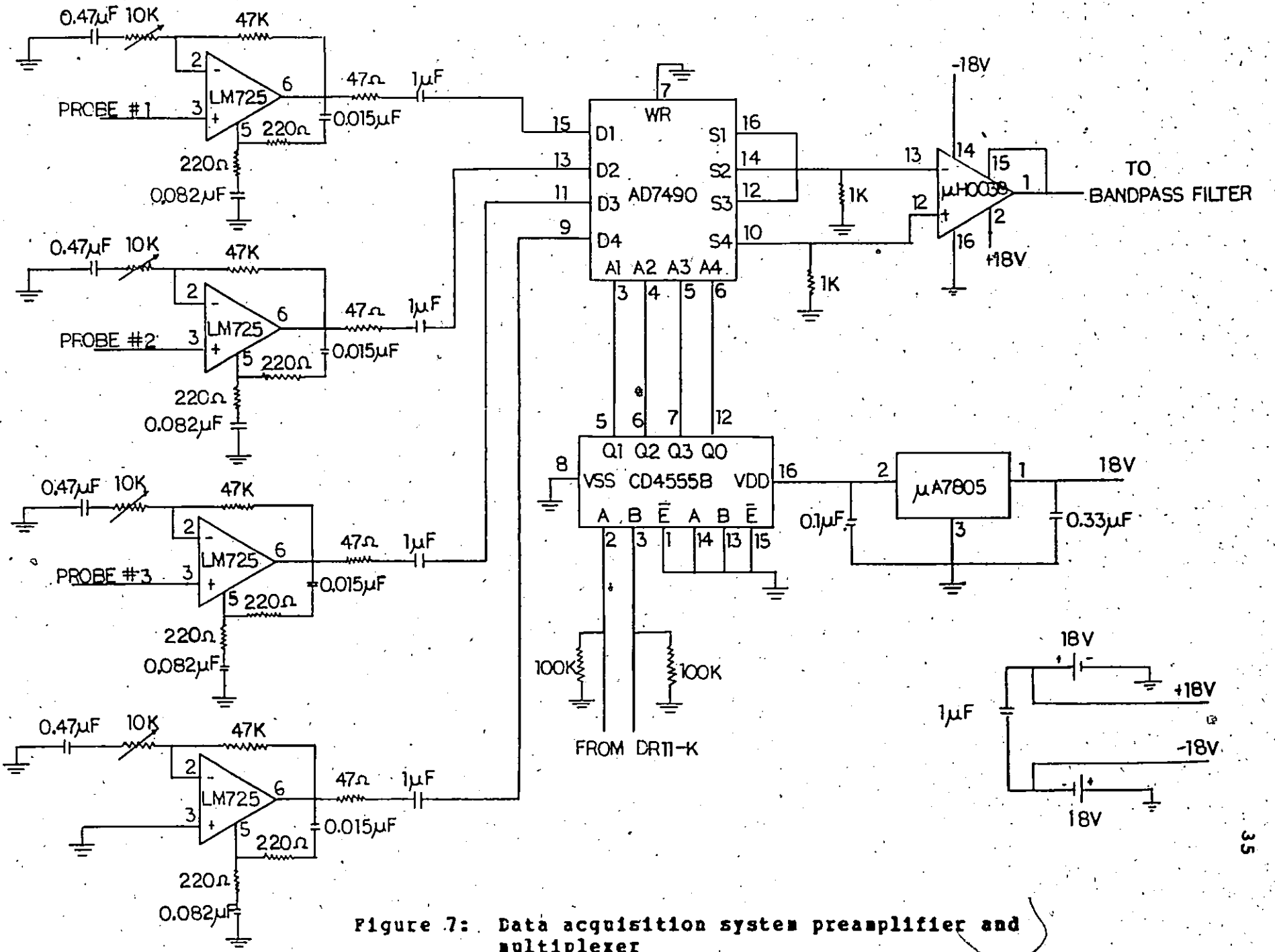

Figure 7: Data acquisition system preamplifier and multiplexer

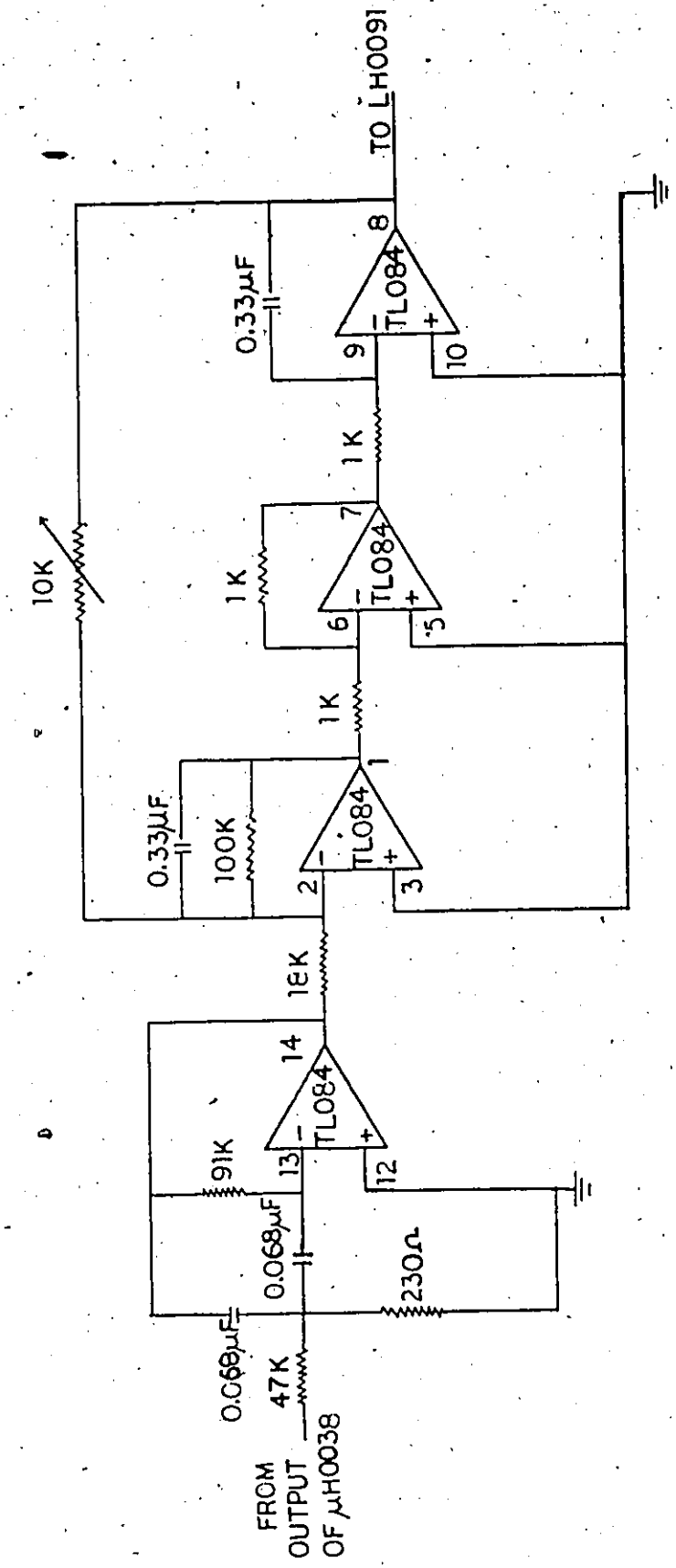

Figure 8: Data acquisition system bandpass filter

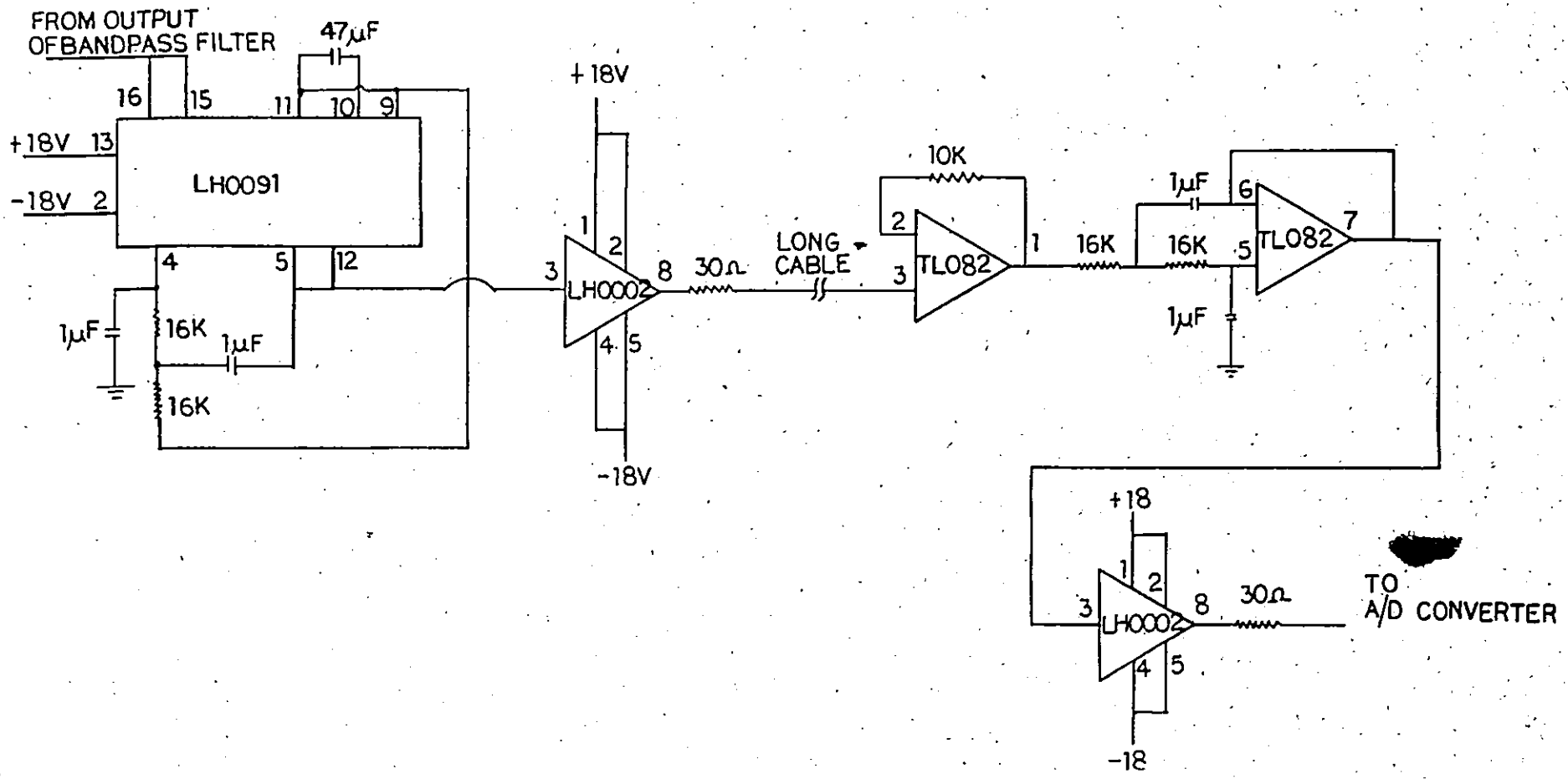

Figure 9: Data acquisition system true RMS to DC converter

This amplifier has a gain variable from 100 to 2000. A bandpass filter with an equivalent Q - factor of 60 and a center frequency of 510 Hz was used. Before the signal is delivered tc the A/D converter via a long cable, it is converted tc DC by a RMS to DC converter (National LH0091).

After prcpagating down the cable, the DC signal passes through a lowpass filter with a cutoff frequency cf about 10 Hz to reject any high-frequency noise. Finally, the signal is digitized by the A/D converter.

IX. Modulating Frequency

To select a proper modulation frequency, the noise characteristic and the frequency response of the probe have to be known. An experimental approach is used to obtain the required information.

(i) Noise characteristic of the probe

Fig. 10 shows a block diagram of an experimental arrangement to obtain the noise characteristic of the probe. A lock-in amplifier is utilized as a narrow band bandpass filter with a variable centre frequency. Its equivalent noise bandwidth is variable and can be as narrow as 1.5 Hz. The experimental results are illustrated in Fig. 11 . It is evident that the maximum occurs at the frequencies which are the odd harmonic of 60 Hz.

(ii) Frequency response of the probe

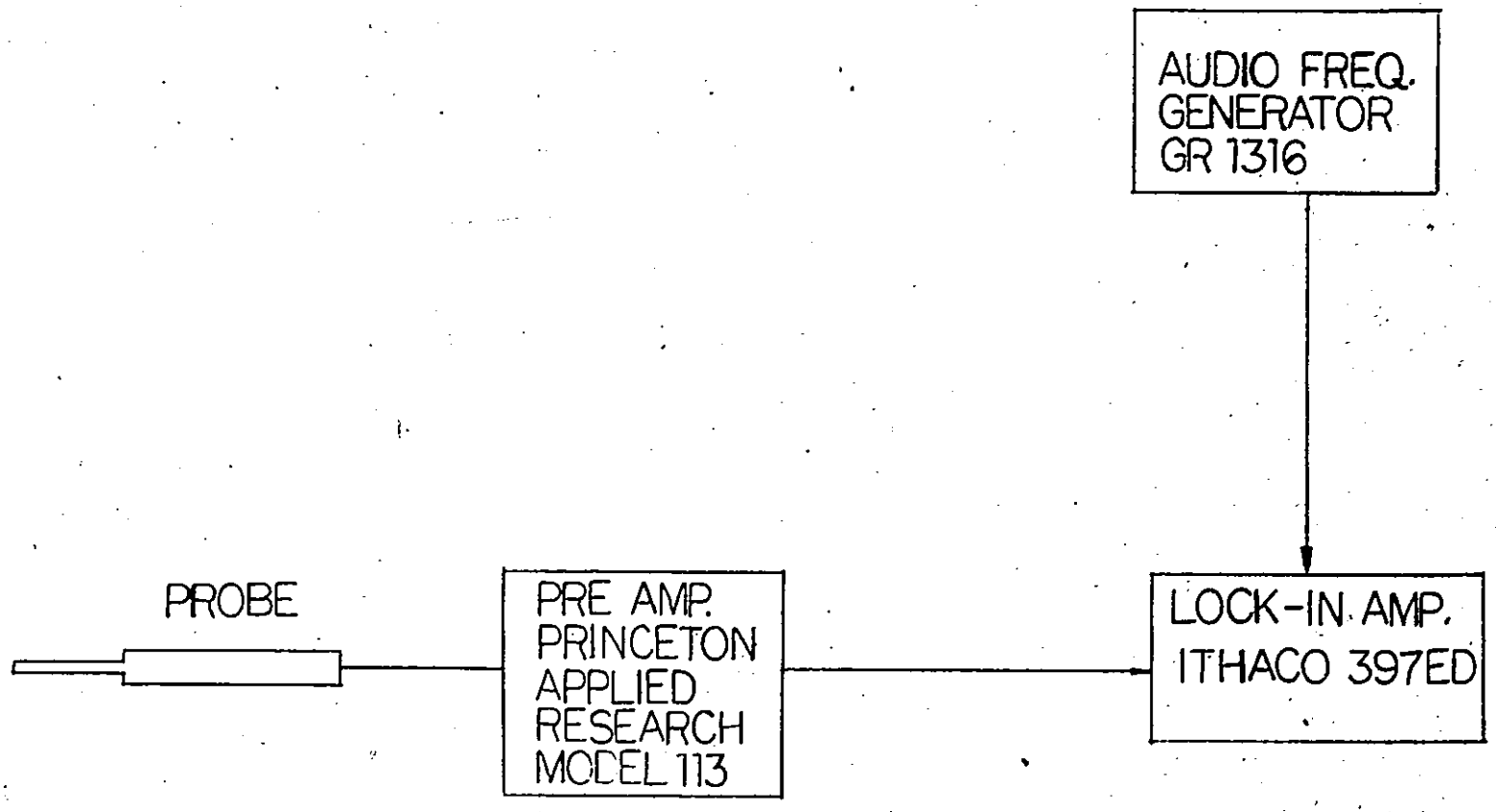

Figure 10: Block diagram for measuring the noise characteristic of the probe

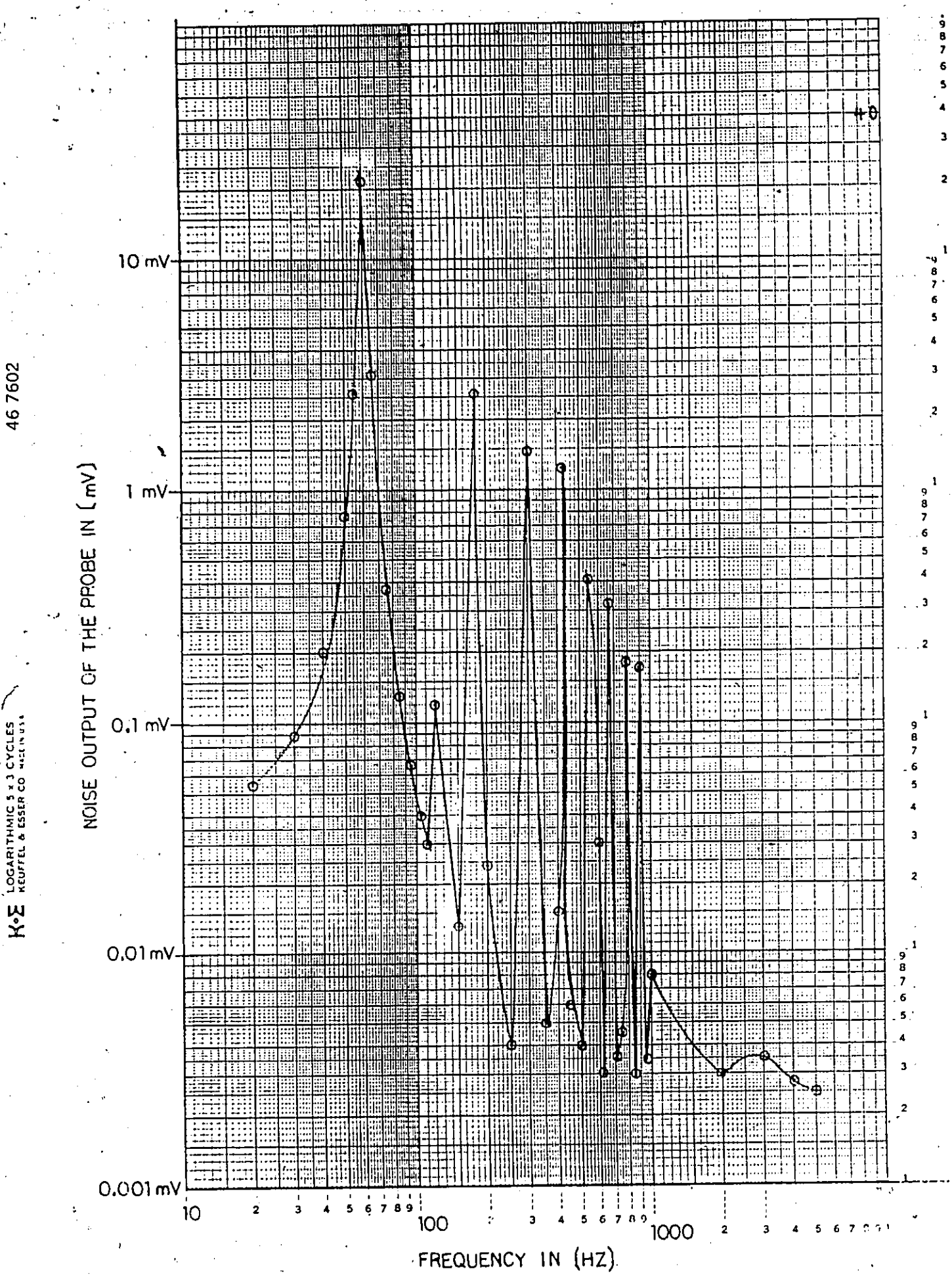

Figure 11: Noise at the output of the probe vs frequency

To obtain the frequency response of the probe, an experimental arrangement shown in Fig. 12 was assembled. The probe was placed in a section of a rectangular waveguide. The amplitude of the output signal from the probe as a function of the modulating frequency is shown in Fig. 13 for the NARDA probe. The signal-to-noise ratio varies only slightly between 300 Hz and 700 Hz. At frequencies above 700 Hz the output signal of the probe drops dramatically. This is due to the characteristic of the probe itself. Its high-resistance thin-film leads create a low-pass distributed filter composed of a highly lossy, series inductance with distributed interlead capacitance [21].

A frequency of 510 Hz which lies between 300 Hz and 700 Hz and is not an odd harmonic of 60 Hz, is chosen as the modulating frequency.

Because of the high Q factor of the bandpass filter, a stable local oscillator has to be chosen. A GR 1316 oscillator with long-term stability of 0.005% (12 hours) was employed.

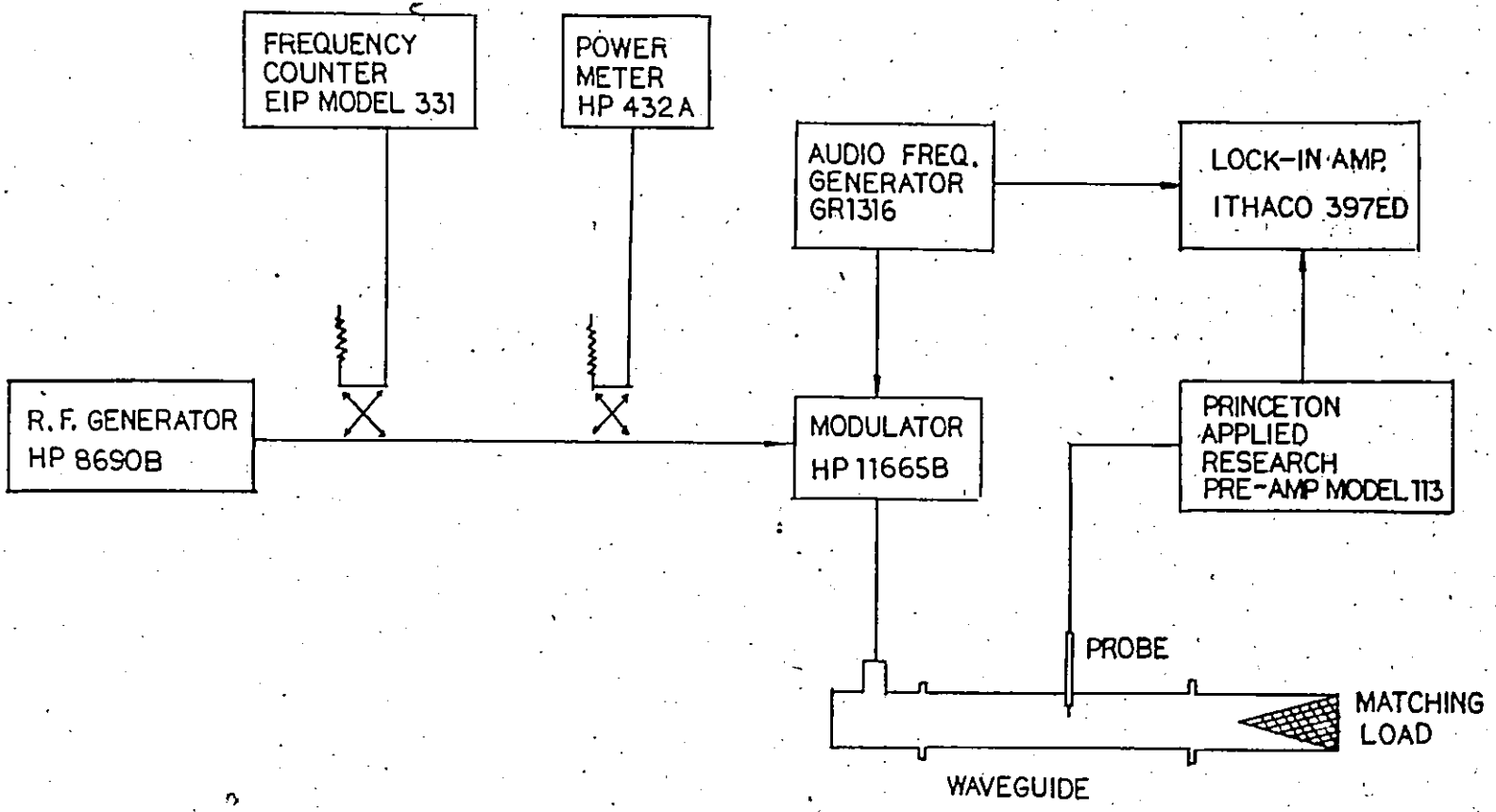

Figure 12: Block diagram for measuring the response of the probe

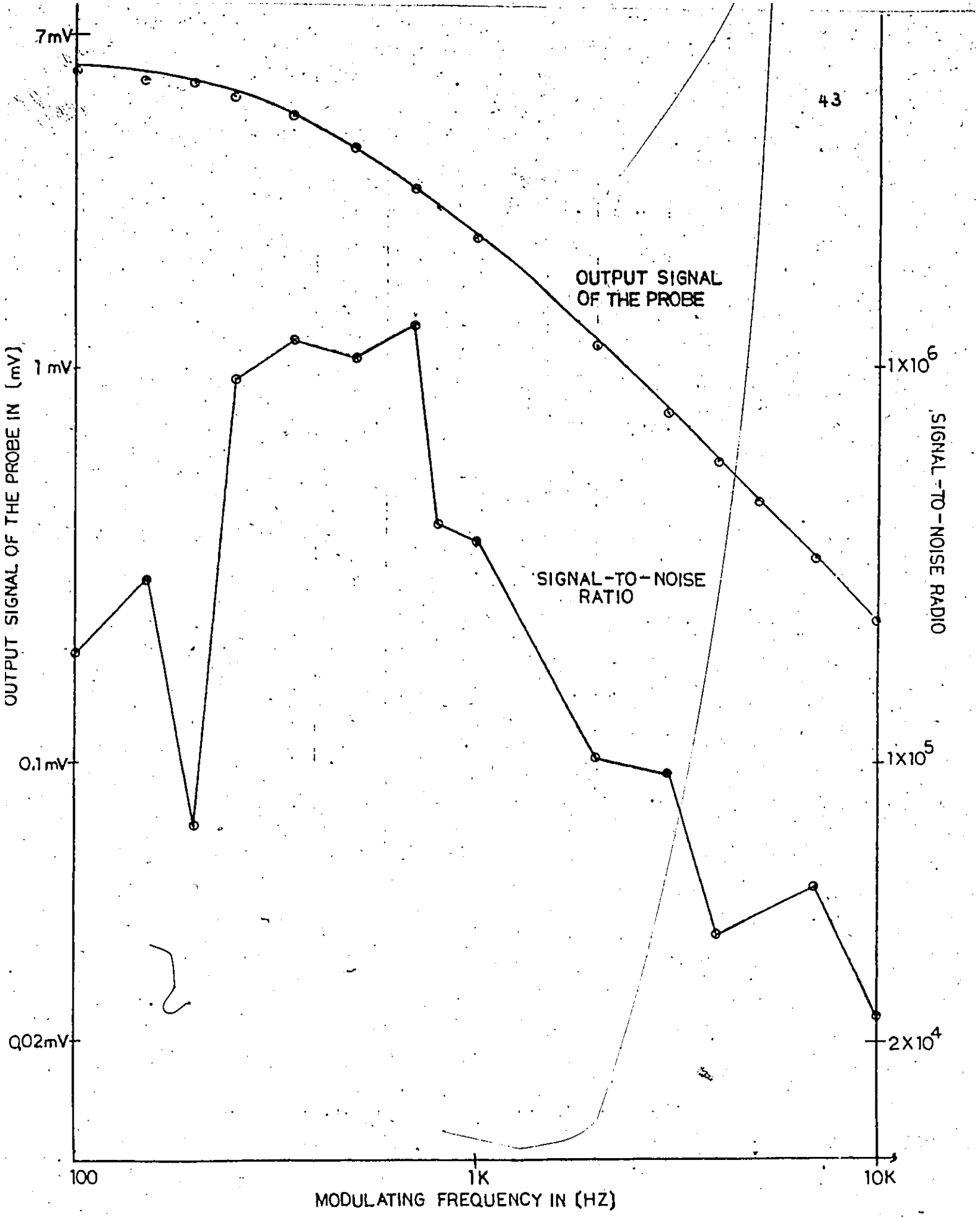

Figure 13: Detected signal from the probe for different modulating frequencies

2.2 SOFTWARE DEVELOPMENT

In this research, the PDP-11 is used for book-keeping and monitoring. At the hole location phase, the PDP-11 stores a map of selected hole locations. In the data collection phase, the computer is able to monitor the scanning system control unit to position the probe in a selected hole and acquire the data.

2.2.1 Storage Map of Hole Location Phase

To store a map of hole locations, a file which is named by an operator is created. After having tested a communication link between the computer and the control unit, the coordinates of each hole transmitted from the control unit are stored on the disk. Up to 200 coordinates of holes plus two reference coordinates can be stored. The reference coordinates are used as an alignment in the data acquisition phase. The depth of each hole is entered from a keyboard by the operator. At the end of this phase, a hardcopy of the map of hole locations is obtained from the line-printer.

2.2.2 Data Collection Phase

After the map of hole locations is stored in the computer memory, the data acquisition phase can be started. At the beginning, the operator selects the name of the data file.

and the name of the hole location map file. The distance intervals along the Z axis are also entered from the keyboard by the operator. The maximum transmission power which is measured by a power meter, is recorded. After having tested the communication link between the computer and the control unit, two reference positions are transmitted to the control unit. These two positions are used to align the phantom model with the map. After the alignment is completed, the operator enters an acknowledgement from the keyboard. The computer starts to monitor the control unit to position the probe in previously selected locations by transmitting the coordinates of the selected hole. To prevent the probe from hitting the surface of the model, an information about the status of the probe is sent back from the control unit. If any of the limit switches is activated, the whole scanning system stops and waits for a command from the operator. The output voltage of the probe normalized to the transmitted power together with the depth of probe is acquired and stored in the computer memory. The field intensity can be computed from the probe output voltage [24]

$$\frac{V_T}{P_t} = \frac{B_m E_T^2}{P_t} \qquad (5)$$

where V_T is the sum of all output voltages of the probe, E_T is the total electric field, P_t is the transmission power (maximun transmitted power X attenuation factor of a computer controlled attenuator), B_m is an empirical constant.

The procedure continues until all the holes are scanned. The flowcharts for both phases are given in appendix A.

2.3 AREAS OF CONTRIBUTION

In this project, the areas which I participated were electronic design and computer programming.

(1) Hardware design

A data acquisition network was designed and implemented. The network consists of an a.c. amplifier, a multiplexer, a bandpass filter and a°R.M.S. converter.

The a.c. amplifier is used to amplify the signal from the probe. It has the voltage gain of 10. The network also contains a high-pass filter with a cutoff frequency of 60 Hz and used to attenuate the frequency components below the line frequency (60 Hz). Since a tri-axial probe is used, three amplifiers are required to amplify the signals from each axis of the probe.

To reduce the amount of circuity, a multiplexer is used instead of three identical systems. The multiplexer is used to select one of three outputs of the a.c. amplifiers to an instrumentation amplifier. It consists of an analog switch (AD7490) and a decoder (CD4555B). The decoder is used in order to reduce the number of digital control lines from the PDP-11. Channel 1, channel 2 and channel 3 are selected by the decoder inputs 01, 10 and 11, respectively.

Before the detected signal is fed to a bandpass filter, to filter out any unwanted frequency components, it is amplified by the instrumentation amplifier (μH0038). The voltage gain of the amplifier is 100.

The bandpass filter is comprised of two cascaded second order active bandpass filters. Their center frequencies are 510 Hz and their Q factors are 10 and 50, respectively. The second stage of the bandpass filter is a biquad bandpass filter type. Although it requires more elements than the first stage, it has very low sensitivity to element changes and is very easy to tune. The purpose of this stage is to provide fine tuning of the center frequency of the bandpass filter. An operational amplifier (TL084) is used to implement the bandpass filter because there are four low cost amplifiers in one package.

Before the wanted signal is delivered to the A/D converter via a long cable, the signal is converted to DC. A

R.M.S. to DC converter (LH0091) which generates a DC output equal to the R.M.S. value of the signal, is used. An additional operational amplifier in the converter is used to implement a second order lowpass filter with a cutoff frequency of about 10 Hz. This filter is used to smooth out the ripple and noise on the DC output of the converter. Finally, the DC signal is fed to a line driver (LH0002) which is used to drive a long cable at low output impedance.

To reduce noise and radio-frequency interference, the electronic components are mounted on the printed circuit board with a ground plane. The circuity of the network is shown in Fig. 7, Fig. 8 and Fig. 9 .

(ii) Computer programming

The programs for the hole location phase and the data collection phase were written. The flowcharts for both phases are shown in appendix A. In the hole location phase, the computer receives the coordinates of the holes from the scanning system control unit and stores them on the disk. In the data collection phase, the computer monitors the scanning system control unit by transmitting the coordinates of the holes and the control data. The measured data at each location are collected and stored on the disk.

In both phases, the coordinates of the holes and control commands are trans itted through a communication link

between the computer and the control unit. The asynchronous mode with a baud rate of 600 is chosen. To prevent transmission errors, a method in which the received data is re-transmitted to the transmitter for checking, is employed. Any errors stop the operation of the scanning system. CIAS universal disk file subprograms (25) are used to arrange the stored data on the disk. They are used because they provide efficient and flexible handing of data to or from the disk.

Bits 9 and 8 of the digital input/output device (model DK11-K) are connected to the channel selector input of the multiplexer. At each selected location, the computer controls the device and scans from channel 1 to channel 3. The A/D converter is initiated to digitize the measured value from each channel. Signal averaging is employed to improve the signal-to-noise ratio. Twenty measured values from each channel are collected and averaged. Finally, the average measured value of each channel is summed up and stored on the disk. The measured value at each location is printed out by the lineprinter.

To avoid small air pockets between the probe tip and the phantom material, the probe is slowly and continuously driven through the phantom model from the top to the bottom at each selected location. Then the probe is withdrawn and moved to another location.

Chapter III

EXPERIMENTAL METHODS AND RESULTS

In this chapter, the testing methods and experimental results for the scanning system and the electronic network are presented. This includes measuring the size of the scanning volume, determining the repeatability of positioning the probe and the response of the data acquisition network. The data storage method are also evaluated.

3.1 SCANNING VOLUME

I. Experimental Method

To measure the maximum scanning volume of the scanning system, the limit switches were moved to the far ends. The scanning system was controlled manually and moved from an upper corner to a diagonal opposite corner. The maximum displacement on each axis was measured using a measuring tape.

II. Results

The maximum displacement in length (X-axis) 1.90m.

The maximum displacement in width (Y-axis) 0.5m.

The maximum displacement in depth (Z-axis) 0.45m.

The maximum scanning volume is $1.9 \times 0.5 \times 0.45\ m^3$

3.2 REPEATABILITY OF THE SCANNING SYSTEM

The repeatability of positioning the probe is an essential parameter of the scanning system. To determine this parameter, the scanning system was repeatedly instructed to locate a particular selected position under computer control.

I. Experimental Method

A sheet of graph paper was placed under the scanning structure within the scanning volume of the system. The probe was replaced with a syringe needle (size 25 gauge) which was used as a marker (Fig. 14). At the beginning, the "manual" mode of the scanning control unit was used and the marker was moved to an arbitrary position within the area of the paper. The coordinates of the position were stored in the computer. Then the "remote" mode was selected. Under the "remote" mode, the computer instructed the control unit to reposition the marker to the selected position. When the marker was over the selected

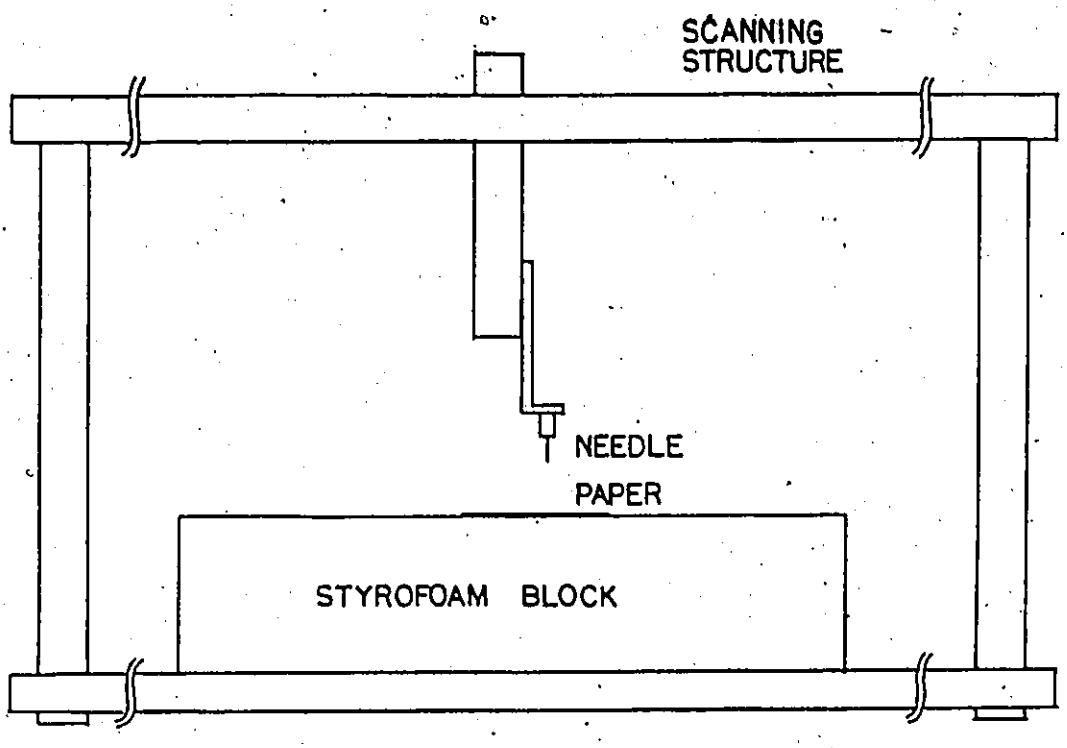

Figure 14: Experimental arrangement for testing the repeatability of the scanning system

position, it was lowered down and made a small hole in the paper. This continued until all the selected positions were scanned. The marker was then returned to its initial position before the second scan could take place. This was repeated nine times. Then the paper was shifted by a few centimeters and scanned only once. Using a microscope, the dimension of the holes which were punched nine times were compared with the dimension of the holes which were punched only once. The difference between the dimensions of those holes was taken as the maximum error in positioning.

To obtain the repeatability of the scanning system in Z axis, the experimental arrangement shown in Fig. 15 was used. The computer directed the scanning system control unit to move carriage about 1 cm. (20 steps) along the Z axis. The displacement was measured by a dial gage indicator. Then the carriage was returned to its initial position and the procedure was repeated. The difference between the maximum displacement and average displacement averaged for a few measurements (0.9682 cm) was taken as the maximum error in positioning in Z axis.

II. Results

Six arbitrary positions are selected for this experiment. After examining the holes under the microscope, the worst one is chosen and enlarged (Fig. 16). By measuring the dimension of the holes, the errors in both X and Y

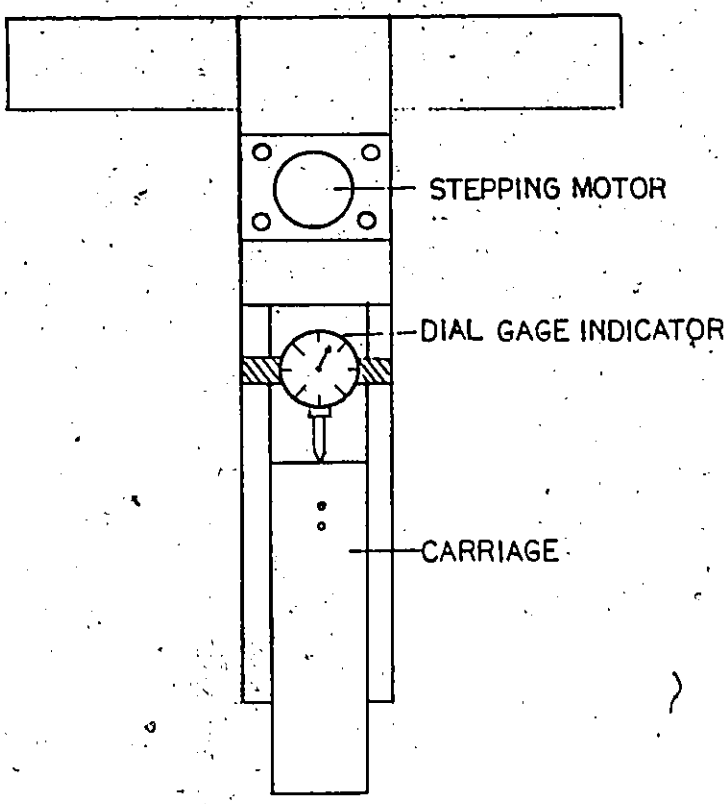

Figure 15: Experimental arrangement for measuring the repeatability of the scanning system in Z axis

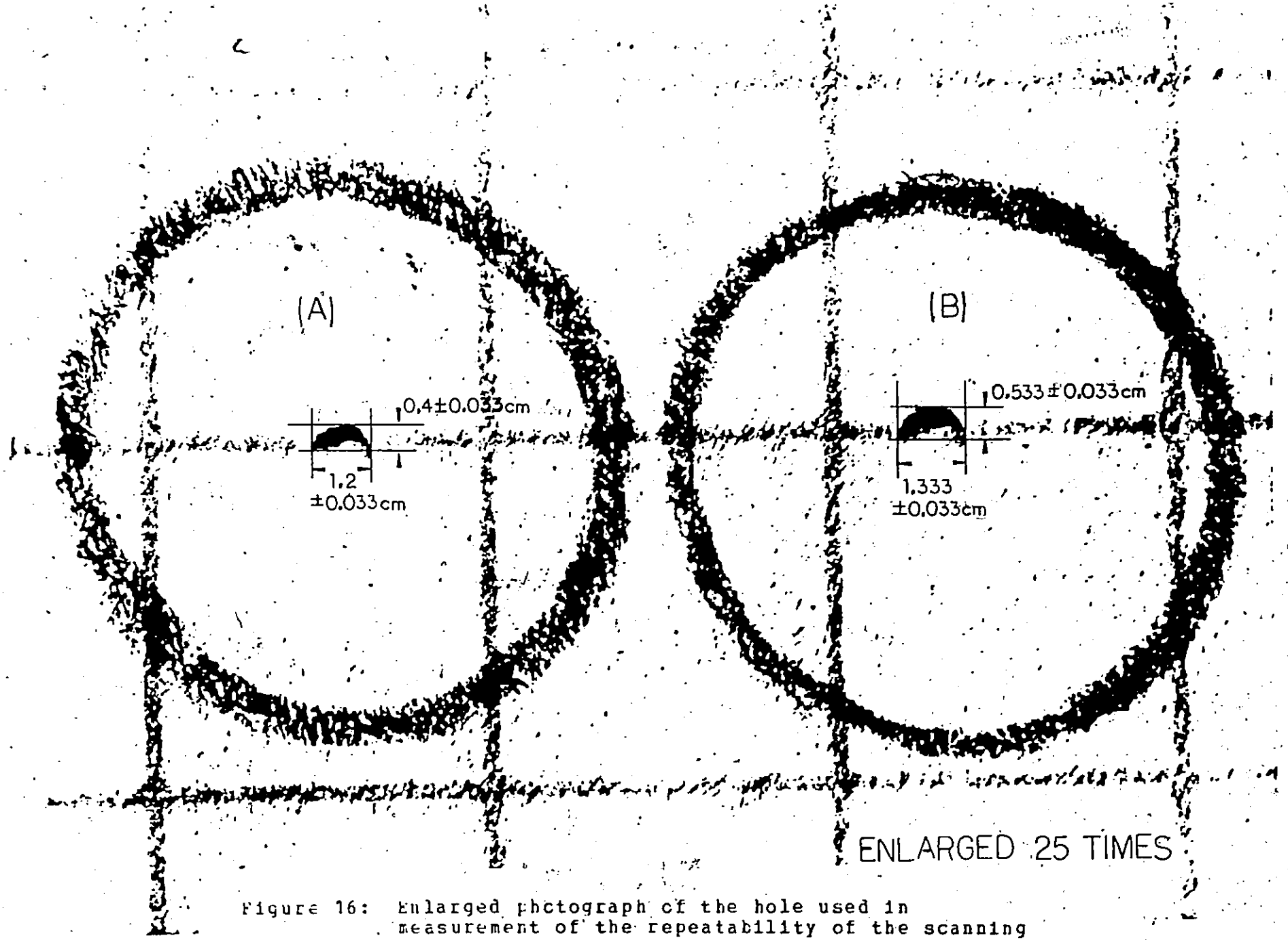

Figure 16: Enlarged photograph of the hole used in measurement of the repeatability of the scanning system

A - hole which is made by one scan
B - hole which is made by nine scans

directions are found to be less than 0.05 mm. The error in this experiment is due to the accuracy of measurement.

For the Z direction, the experimental results are shown in table 2 . The measurement error is due to the accuracy in reading the dial gage. The other errors along the Z axis are due to the positioning of the limit switch. This causes the carriage to stop within one motor step of the desired position. Since one motor step in Z direction is equivalent to a displacement of 0.051 cm, this is the maximum error.

3.3 RESPONSE OF THE DATA ACQUISITION NETWORK

The data acquisition network is used to process the output signals from the probe which is proportional to the input power. If the network is linear, the output signal from the network is proportional to the input power. An experimental setup shown in Fig. 17 was used to evaluate the linearity of the data aquisition network.

I. Experimental Method

A detector with a point-contact diode was used to simulate the detector inside the probe. The R.F. generator was set at 0.7 GHz, and the modulation frequency generator at 510 Hz, which was the centre frequency of the bandpass filter of the data acquisition network. By varying the

Table 2. Experimental results for the repeatability of positioning in Z axis

Reference(in.)	Dial gage reading(in.)	Distance travel(in.)
0.0995	0.4805	0.3810
0.0995	0.4807	0.3812
0.0995	0.4807	0.3812
0.0995	0.4807	0.3812
0.0995	0.4807	0.3812
0.0995	0.4807	0.3812
0.0995	0.4808	0.3813
0.0995	0.4807	0.3812
0.0995	0.4808	0.3813
0.0995	0.4808	0.3813
	Means	0.3812 (0.9682 cm)

Maximum error in position = MAX | means - distance travel |
= 0.3812 in. - 0.3810 in.
= 0.0002 in. (0.0005 cm)

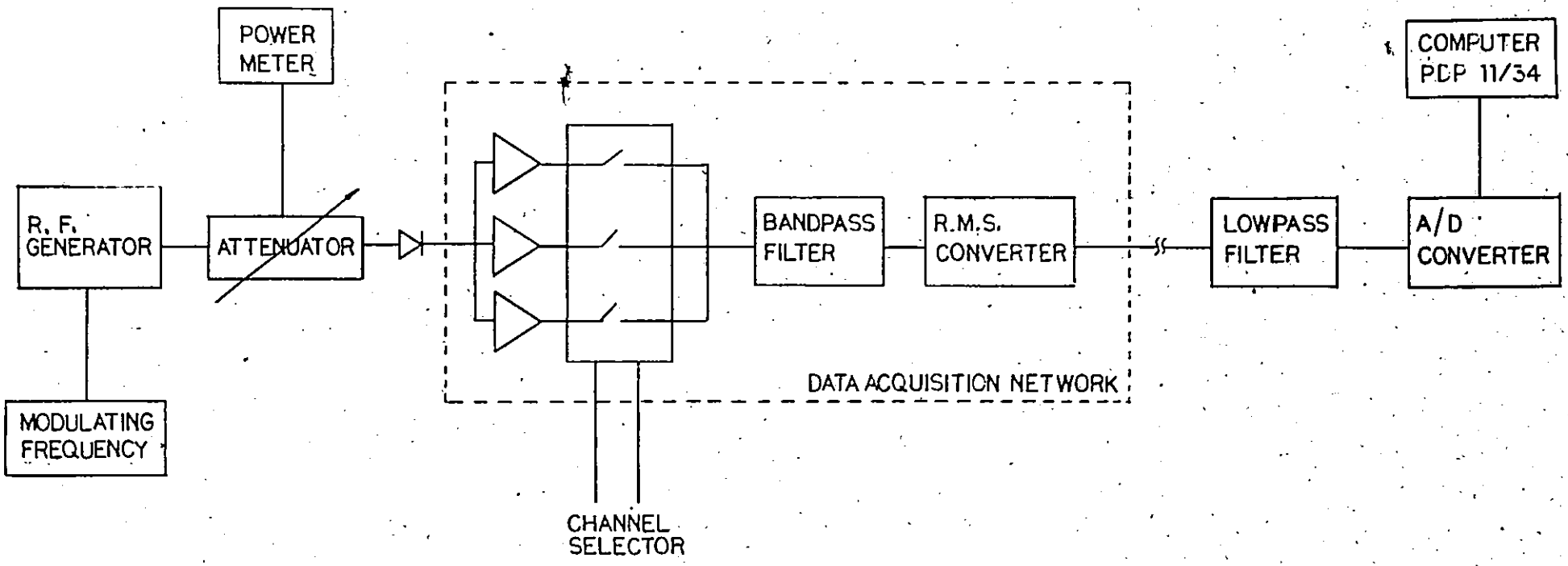

Figure 17: Experimental arrangement for measuring the response of the data acquisition network

attenuator, the input power at the diode detector was changed. By measuring the input power with a power meter and the output voltage of the network, the relationship between output voltage and the input power was obtained. The uncertainty in the power measurement depended upon the uncertainty of the power meter which was ±0.5% of the measured value. The uncertainty of output voltage depended upon the uncertainty of the A/D converter which was ± 2.44 mV.

II. Result

The experimental results are shown in Fig. 18 . At low input power level, the non-linearity is evident. This is due to the non-linearity of the amplifier and the R.M.S. converter. Using the method of least squares [26], the experimental data within a certain range can be approximated by a straight line. The maximum non-linearity (ΔY) within that range is obtained by

$$\Delta Y = \underset{i=1}{\overset{N}{MAX}} |Y_i - y_i| \qquad (6)$$

where Y_i are the experimental points for various x_i, y_i are the points on the straight line for various x_i, i is an integer 1,2,.....N.

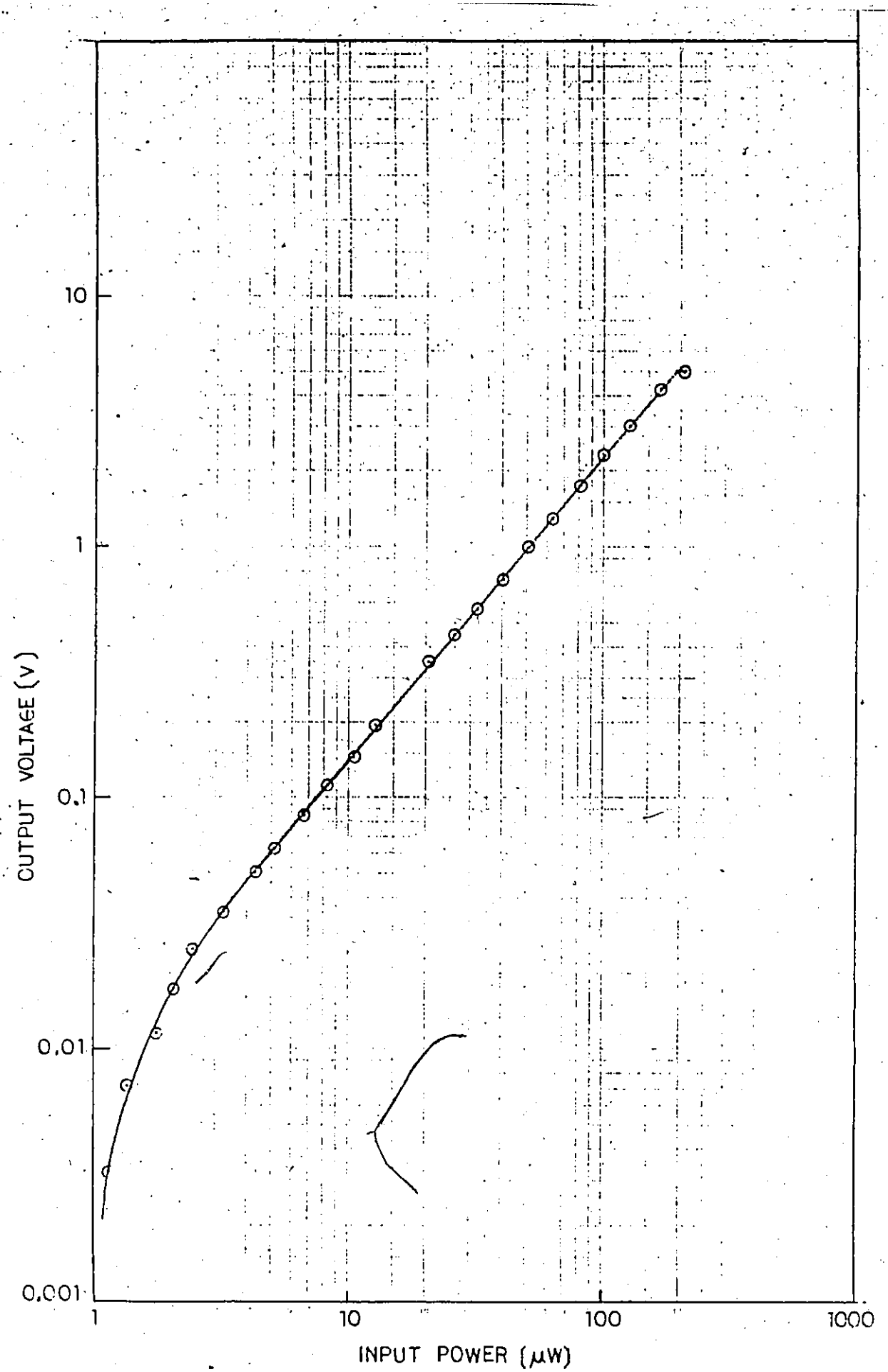

Figure 18: Output voltage from the data acquisition network as a function of the input power

Taking a range from 1.7 μW and 167 μW (about 2 decades), the maximum non-linearity is less than 3% of the full scale, while from 12 μW to 16.7 μW (about 1 decade), the maximum non-linearity is less than 0.3% of the full scale.

3.4 DATA STORAGE

To test the data storage system, the scanning system was used to scan the area in the far-field of a half-wavelength dipole. The half-wavelength dipole was used because its far-field pattern could be calculated theoretically (appendix B).

I. Experimental method

To obtain experimentally the power pattern of a dipole antenna in the far-field, an arrangement shown in Fig. 19 was assembled. A dipole operating at 1.25 GHz, was placed under the scanning structure. The minimum distance between the antenna and the scanning structure was about 10 cm. A RF generator operating at 1.25 GHz, was modulated in amplitude at a frequency 510 Hz. A single axis probe with a zero-bias Schottky diode detector was used to detect the intensity of the RF signal. Initially, a scanning area of 35 cm X 40 cm with 72 locations was used. Each location is 5 cm. apart from its neighbors. The antenna was positioned at the centre of the scanning area. The system was monitored by the computer in "remote" mode. The probe was positioned

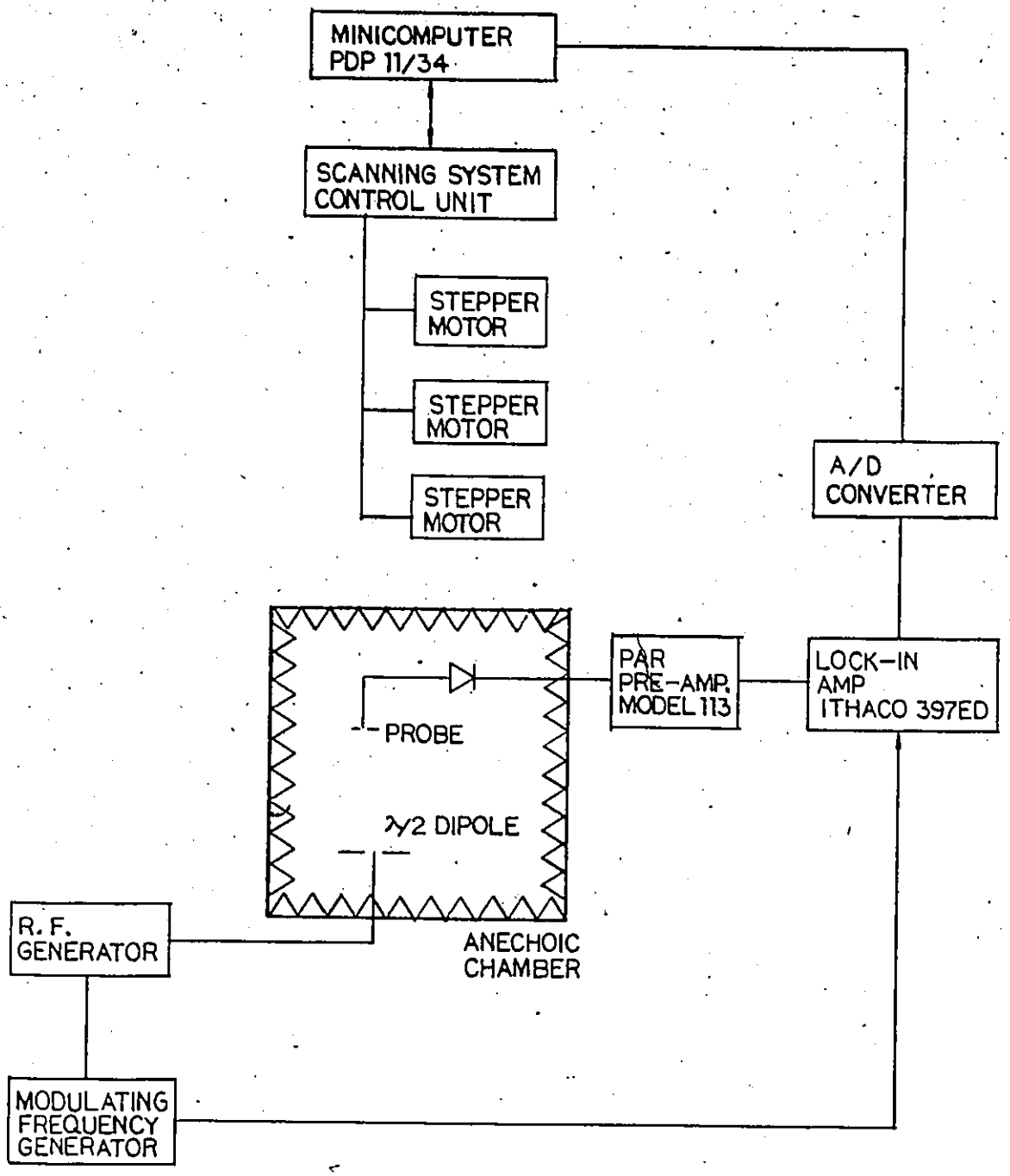

Figure 19: Experimental arrangement for mapping the power pattern of an antenna in the far field zone

in a selected location. The square of the electric field at that location was measured, digitalized and stored in the computer. This continued until all selected locations were scanned. Finally, the stored data were printed out.

II. Result

For the 1.25-GHz dipole antenna, the minimum distance required to meet the far-field condition, is about 12 cm. The relative power pattern at a distance of 18 cm from the antenna is calculated (Fig. 20). The maximum of the field occurs at the centre. The output signals from the probe at the same distance from the antenna is shown in Fig. 20 . The maximum of the signal is slightly off the centre. This is due to the errors in positioning of the antenna during the experiment. The general pattern of the field agrees quite well with the calculation.

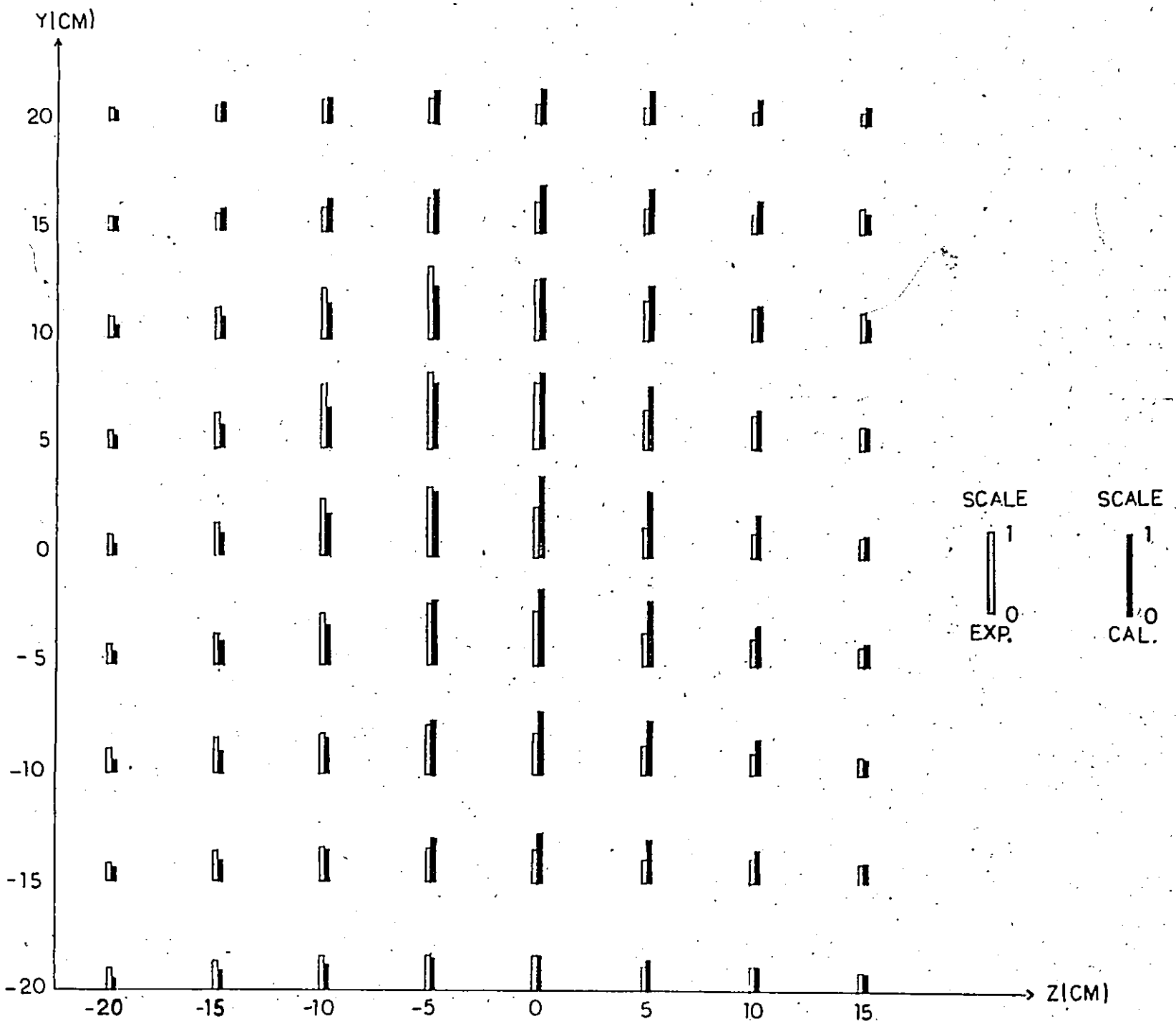

Figure 20: Theoretical and experimental field patterns of a half-wavelength antenna at 18 cm from the antenna

Chapter IV

CONCLUSION AND DISCUSSION

In this chapter, a summary of the experimental results of the scanning system is presented and some suggestions for future development of the system are discussed.

4.1 CONCLUSIONS

The experimental results demonstrate that the computer-controlled scanning system meets the specifications presented in the Chapter 1.

(i) Scanning volume

The scanning volume of the scanning system is 1.9 X 0.5 X 0.45 m^3. It is large enough to scan full scale simulated biological bodies, such as a human body irradiated by selected sources in both far and near field.

(ii) Repeatability of the scanning system

Repeatability of a particular selected position was found to be better than 0.05 mm in both X and Y direction. In Z direction, the repeatability was found to be better than 0.5 mm. To minimize the errors, operation in the half-step mode is recommended. This gives finer system resolution, but is

slower. In fact, the repeatability of positioning is more than sufficient for the purpose of this research.

(iii) Linearity of the data acquisition system

The linearity of the data acquisition system depends on the dynamic range of operation. Since a computer-controlled attenuator is employed, the dynamic range of the network is quite wide. One decade range (input power from 12 μW to 167 μW) is recommended. This gives the maximum non-linearity less than 0.3% of the full scale.

(iv) Data storage

Examination of the field distributions of a half-wavelength dipole presented in chapter 3 indicates that the data storage system is working satisfactorily. The stored data are arranged in such a way that they are easily addressed and displayed. At present, the data are printed out by a line-printer. When a X-Y plotter becomes available, the data can be recorded in a graphical form.

4.2 SUGGESTIONS FOR FUTURE DEVELOPMENT

For future development of the scanning system, the following suggestions are given and discussed.

(i) Electrical burnout

The tri-axial probe is easy to burn out. Some precautions are necessary in handling the probe. The probe should never be exposed to any radiation sources when it is not connected to the data acquisition network with power on. High level radiation sources also cause the electrical burnout. A computer controlled attenuator should be set at maximum attenuation when the probe is in the air or close to the radiation sources.

(ii) Radio frequency interference

Radio frequency interference (RFI) problems occur in instruments using a detector diode to convert radiowaves or microwaves to low-frequency or DC signals [21] [22]. This interference may impair the performance of the electronic system by increasing the noise level and acting as a false information signal. Proper shielding techniques [29] [30] should be employed to minimize the amount of interference. At present, the network was placed inside a diecast box surrounded with abscrbing materials to reduce the amount of interference.

(iii) Scattering from metal cables

Metal cable, such as RG 58/U shielded coaxial cable, in the test field, can cause scattering [21] [22]. In order to eliminate scattering by cables, an optical fibre system is recommended. An optical fibre system which consists of a

transmitter, receiver and an optical fibre, can be used to replace the cable between the output of the data acquisition network and the input to the A/D converter.

Switching transients can also cause the electrical burn-out of the probe when the computer selects one of the data channels. An optical fibre link between the channel selector and the digital output is also recommended.

(iv) Data display

Since the electromagnetic energy absorption is also dependent on the orientation of the electric fields, the information on three orthogonal components of the electric field vector is very useful. By modifying the computer program, the measurement results from each axis of the probe can be stored separately. To display these data, a special system has to be developed. The "hockeypucks" method [31] has been suggested for this purpose. The method involves arrowheads in form of short cylinders (hockeypucks) to display the orientation and the intensity of vector fields at various locations.

(V) Probe calibration

The response of the probe is depended on the dielectric constant of the medium in which the measurements are being made [18] [20]. By calibrating the probe at a particular frequency, this effect can be eliminated [24].

Appendix A

FLOWCHART OF THE SCANNING SYSTEM

The software developement of the scanning system includes:

i) Hole map storage mode.

ii) Data collection mode.

The flowcharts of each mode are shown below.

Flovchart of the storage a map of hole location session

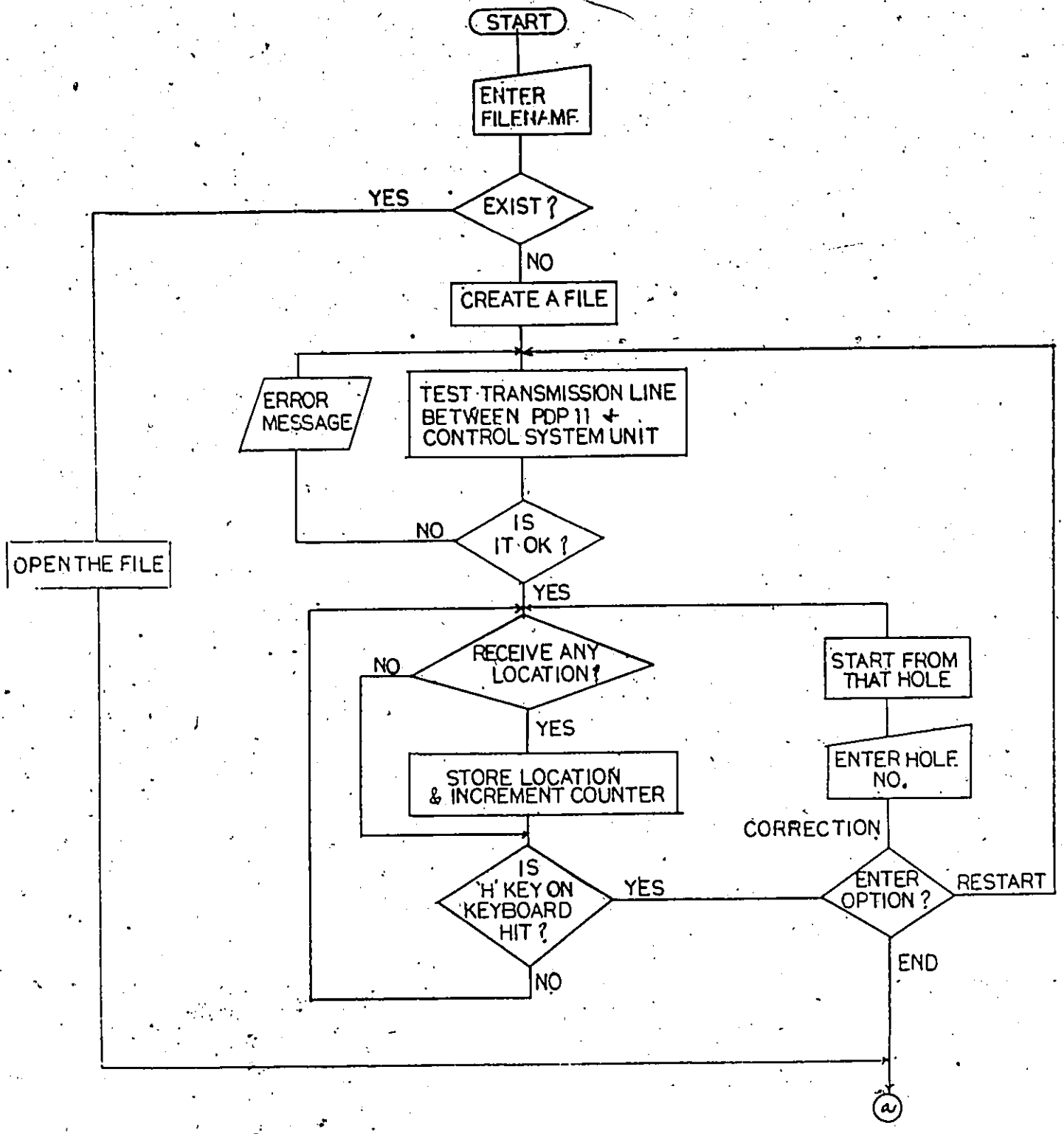

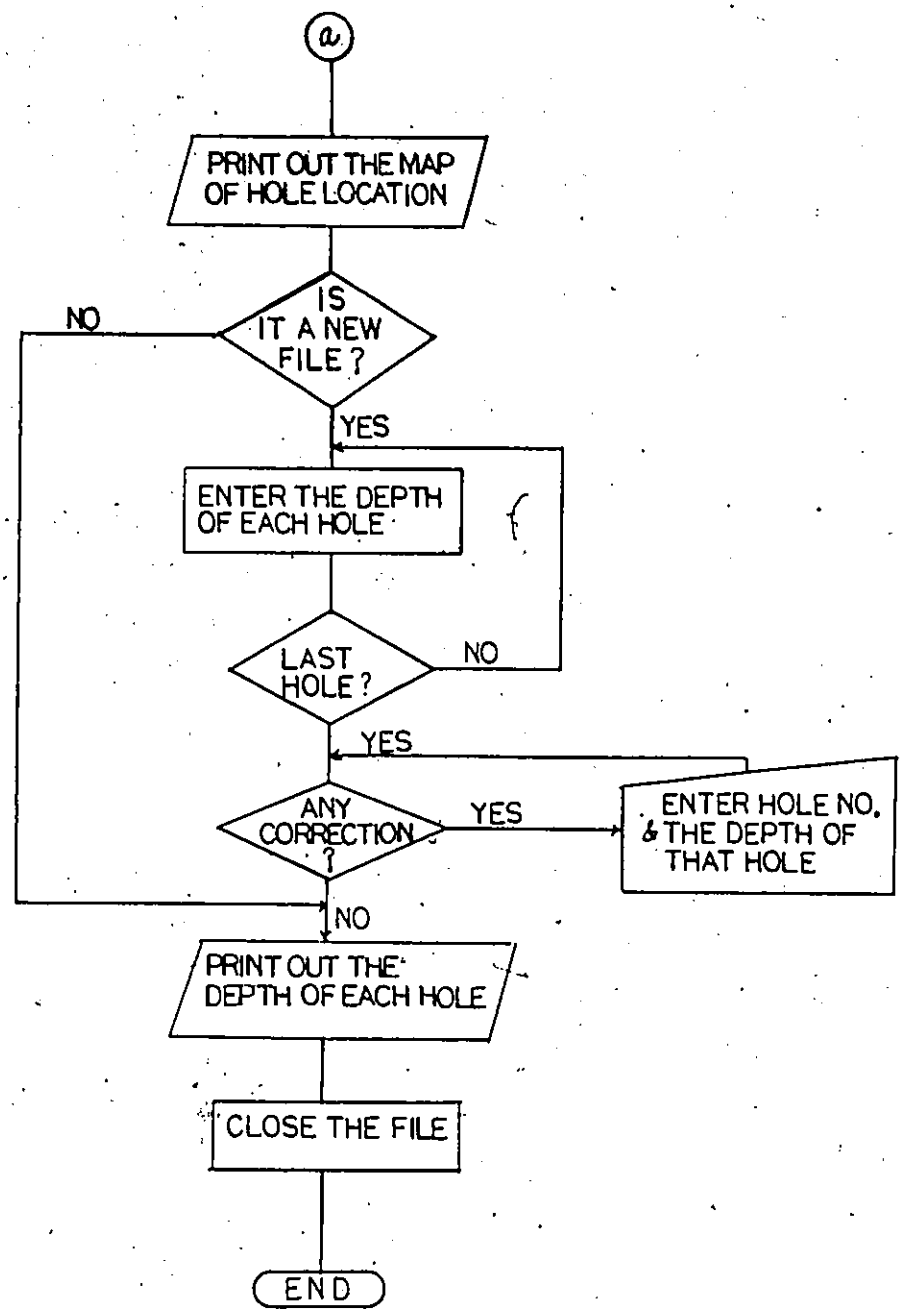
a
PRINT OUT THE MAP OF HOLE LOCATION
IS IT A NEW FILE ?
NO
YES
ENTER THE DEPTH OF EACH HOLE
LAST HOLE ?
NO
YES
ANY CORRECTION ?
YES
ENTER HOLE NO. & THE DEPTH OF THAT HOLE
NO
PRINT OUT THE DEPTH OF EACH HOLE
CLOSE THE FILE
END

. Flowchart of the data collection session

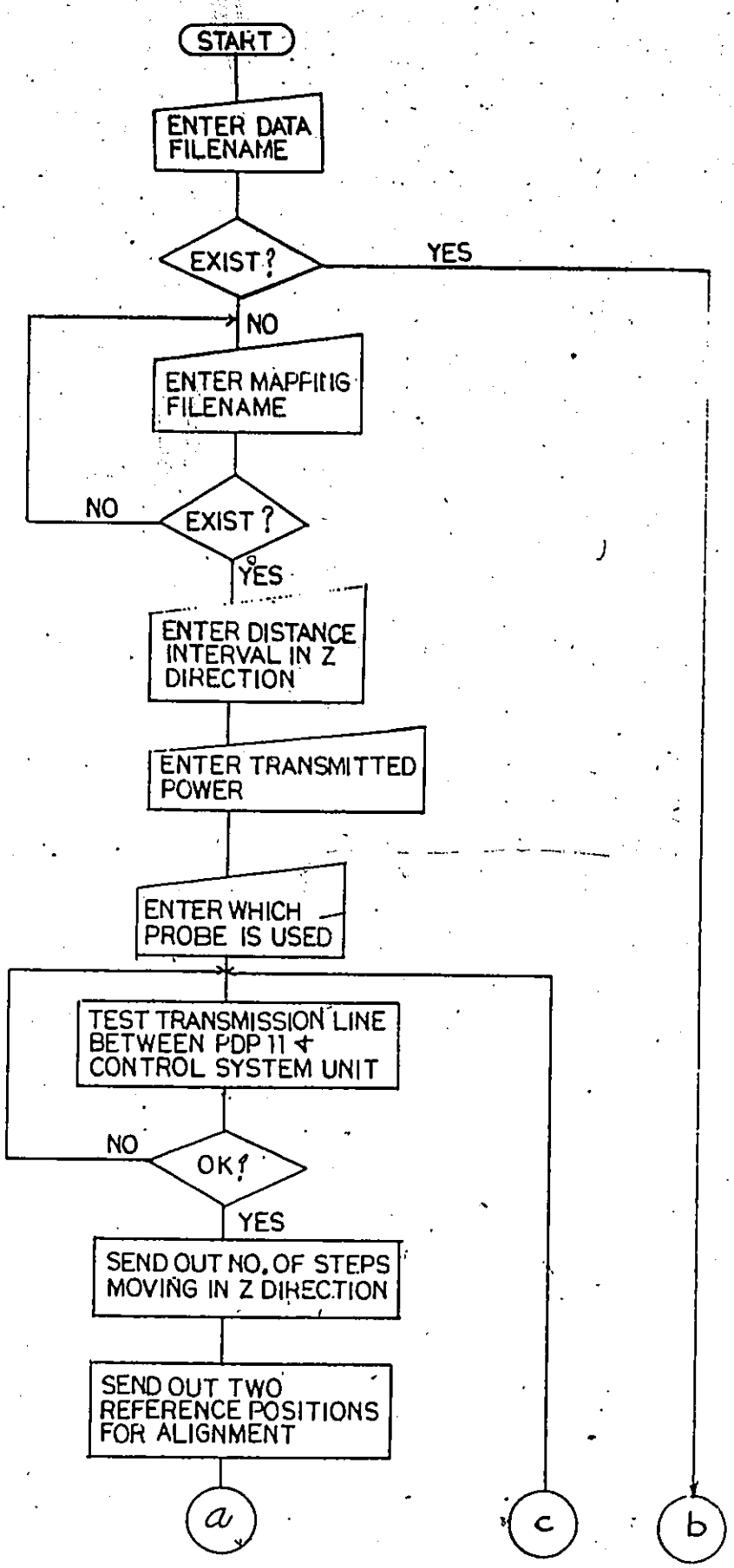

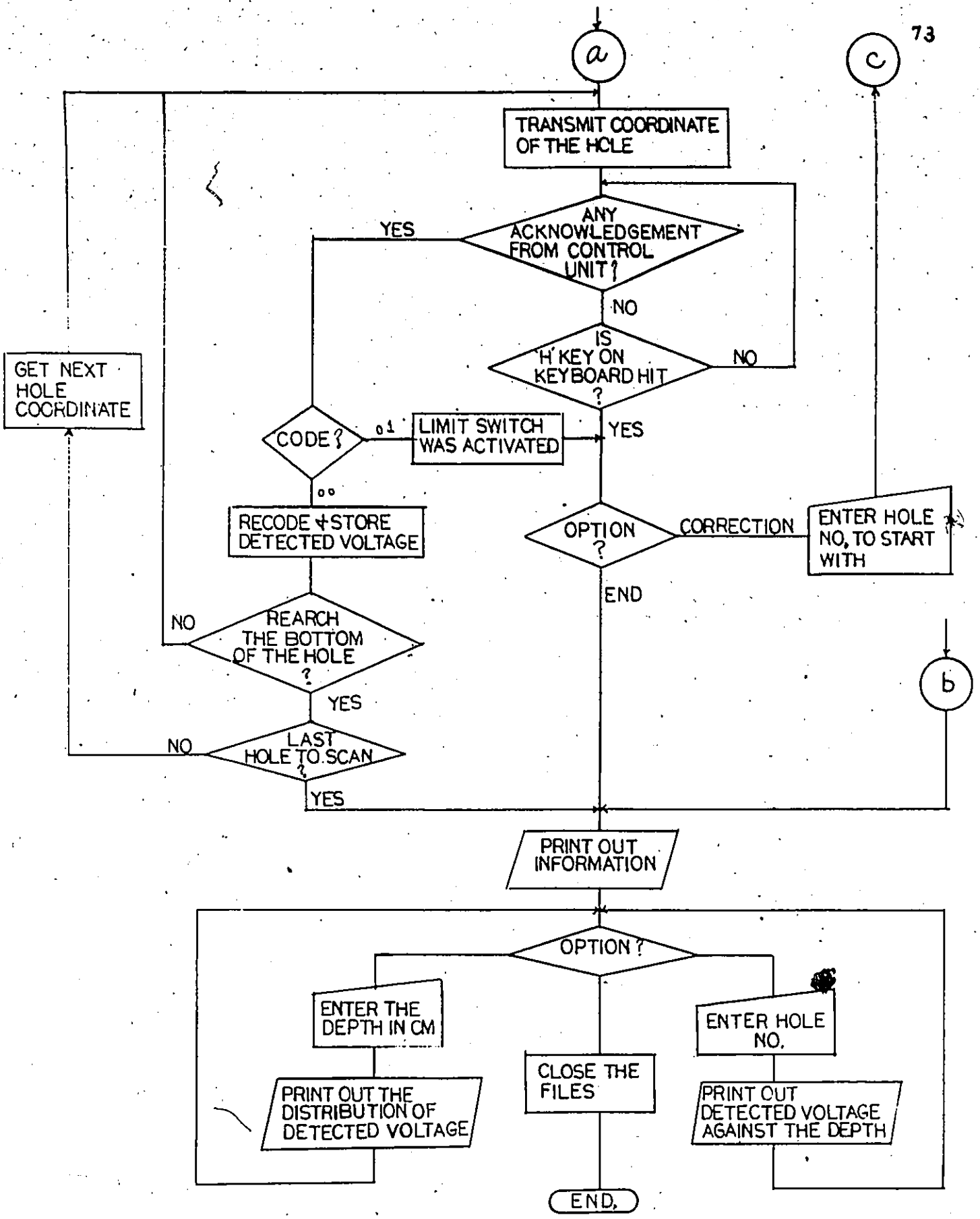
a
c
TRANSMIT COORDINATE OF THE HOLE
ANY ACKNOWLEDGEMENT FROM CONTROL UNIT?
YES
NO
IS 'H' KEY ON KEYBOARD HIT ?
NO
YES
GET NEXT HOLE COORDINATE
CODE?
01
LIMIT SWITCH WAS ACTIVATED
00
RECODE & STORE DETECTED VOLTAGE
OPTION ?
CORRECTION
ENTER HOLE NO, TO START WITH
END
NO
REARCH THE BOTTOM OF THE HOLE ?
YES
NO
LAST HOLE TO SCAN ?
YES
b
PRINT OUT INFORMATION
OPTION ?
ENTER THE DEPTH IN CM
PRINT OUT THE DISTRIBUTION OF DETECTED VOLTAGE
CLOSE THE FILES
ENTER HOLE NO.
PRINT OUT DETECTED VOLTAGE AGAINST THE DEPTH
END.

Appendix B

THEORETICAL CALCULATION OF THE HALF-WAVELENGTH DIPOLE RADIATION PATTERN IN THE FAR FIELD

The E_ϕ and E_θ components of the electric field of a half-wavelength dipole at a large distance r (Fig. 21) are [27]

$$E_\theta = \frac{j60[I_o]}{Y}\left[\frac{\cos(\pi/2\cos\theta)}{\sin\theta}\right] \qquad (7)$$

$$E_\phi = 0 \qquad (8)$$

where $[I_o]$ is the current distribution. The total electric field becomes

$$E_T = \sqrt{E_\theta^2 + E_\phi^2} \qquad (9a)$$

$$= E_\theta \qquad (9b)$$

The relation between the average Poynting vector and the electric field at a point of the far field are

$$P_T = \frac{1}{2}\frac{E_T^2}{Z_o} \qquad (10)$$

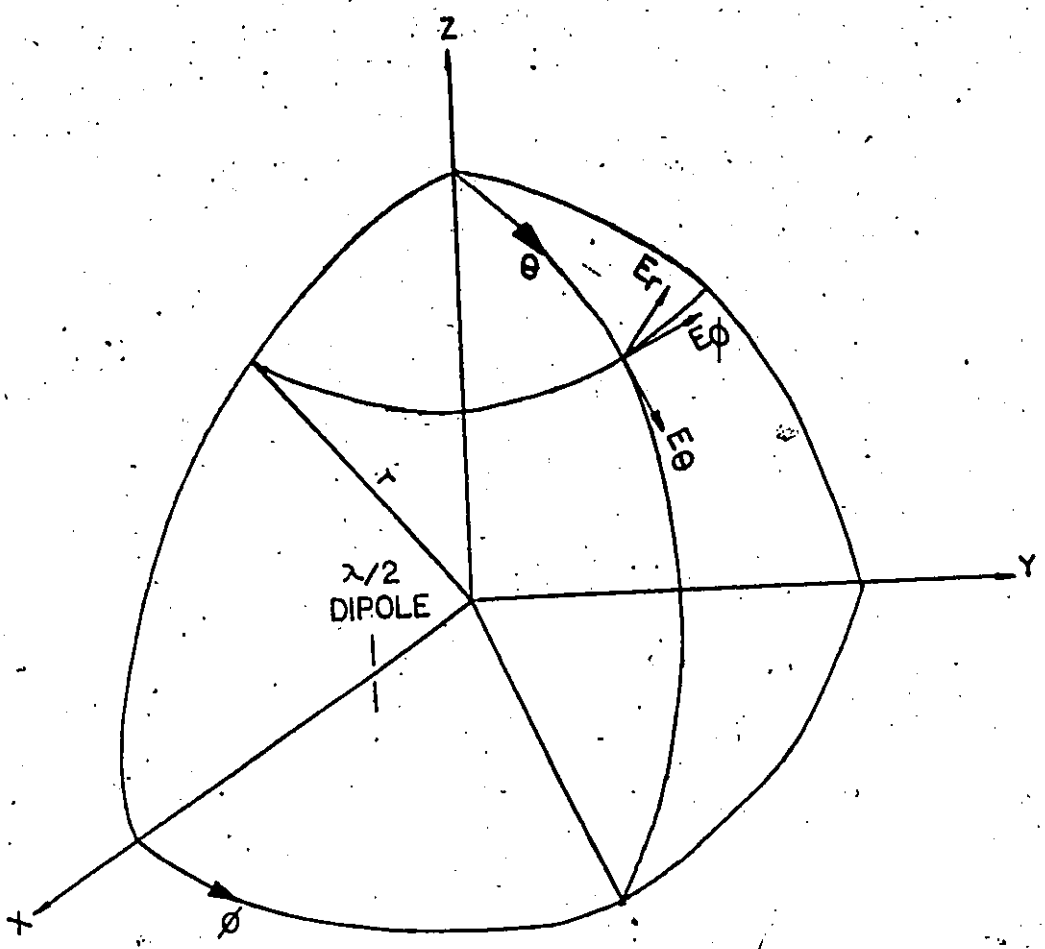

Figure 21: Antenna coordinates

where Z_o is the intrinsic impedance of free-space. For the dipole antenna, the average Poynting vector is

$$P_r = \frac{E_\theta^2}{2Z_o} \qquad (11a)$$

$$= \frac{1}{2Z_o}\left\{\frac{j60[I_o]}{r}\left[\frac{\cos(\pi/2\ \cos\theta)}{\sin\theta}\right]\right\}^2 \qquad (11b)$$

After transformation from the spherical to the rectangular coordinates [28], equation (11) becomes

$$P_r = \frac{1}{2Z_o}\left[\frac{j60[I_o]}{\sqrt{X^2+Y^2+Z^2}}\left(\frac{\cos\pi/2\ \frac{Z}{\sqrt{X^2+Y^2+Z^2}}}{\sin\left(\cos^{-1}\frac{Z}{\sqrt{X^2+Y^2+Z^2}}\right)}\right)\right]^2 \qquad (12)$$

To calculate the power pattern in the far-field, the distance d from the dipole antenna should be at least $d > 2D/\lambda$ where D is the maximum dimension of the antenna and λ is the wavelength. The relative total power pattern in the far-field becomes

$$\frac{P_r}{P_{r\,max}} = \left\{\frac{d}{\sqrt{d^2+Y^2+Z^2}}\left[\frac{\cos\left(\frac{\pi}{2}\ \frac{Z}{\sqrt{d^2+Y^2+Z^2}}\right)}{\sin\left(\cos^{-1}\frac{Z}{\sqrt{d^2+Y^2+Z^2}}\right)}\right]\right\}^2 \qquad (13)$$

REFERENCES

1. Lerner,E.J., "RF radiation : Biological Effects", IEEE Spectrum, Vol. 17, No.12, Dec. 1980, pp. 51-59.

2. Michaelson,S.M., "Microwave Biological Effects: An Overview", Proc. IEEE, Vol. 68, No.1, Jan. 1980, pp.40-49.

3. Mcree,D.I., "Soviet and Eastern European Research on Biological Effects of Microwave Radiation", Proc. IEEE, Vol. 68, No.1, Jan. 1980, pp.84-91.

4. Gandhi,O.P., "State of the Knowledge for Electromagnetic Absorbed Dose in Man and Animals", Proc. IEEE, Vol. 68, No.1, Jan. 1980, pp. 24-25.

5. Iskander,M.F. and Durney,C.H., "Electromagnetic Techniques for Medical Diagnosis: A Review", Proc. IEEE., Vol. 68, No.1, Jan. 1980, pp. 126-132.

6. Short,J.G. and Turner,P.F., "Physical Hyperthermia and Cancer Therapy", Proc. IEEE., Vol. 68, No.1, Jan. 1980, pp. 133-142.

7. Durney,C.H., "Electromagnetic Dosimetry for Models of Humans and Animals: A Review of Theoretical and Numerical Techniques", Proc. IEEE, Vol. 68, No.1, Jan. 1981,pp. 33-40.

8. Walker,P.F. and Bowman,R.R., "Quantifying Hazardous Electromagnetic Fields: Scientific Basis and Practical Considerations", IEEE Trans. Micro. Theory and Techn., Vol. MTT-19, No.2, Feb. 1971, pp. 178-187.

9. Cheung,A.Y. and Koopman,D.W., "Experimental Development of Simulated Biomaterials for Dosimetry Studies of Hazardous Microwave Radiation",IEEE. Tran. on Micro. Theory and Tech., Oct. 1976, pp 669-670.

10. Guy,A.W., "Analysis of Electromagnetic Fields Induced in Biological Tissues by Thermographic Studies on Equivalent Phantom Models",IEEE Trans. on Micro. Theory and Tech., Vol. MTT-19, No.2, Feb. 1971, pp. 205-214.

11. Guy,A.W., Webb,M.D. and Sorensen,C.C., "Determination of Power Absorption in Man Exposed to High Frequency Electromagnetic Fields by Thermographic Measurements on Scale Models", IEEE Trans. on Bio. Eng., Vol. BME-23, No. 5, Sept. 1976, pp. 361-371.

12. Lin,J.C., Guy,A.W. and Kraft,G.H., "Microwave Selective Brain Heating",Journal of Microwave Power, Aug. 1973, pp. 275-286.

13. Guy,A.W., "Electromagnetic Fields and Relative Heating Patterns Due to a Rectangular Aperture Source in Direct Contract with Bilayered Biological Tissue", IEEE Trans. on Micro. Theory and Tech., Vol. MIT-19, No.2, Feb. 1971, pp. 214-224.

14. Allen,S.J. Hurt,W.D., Krupp,J.H., Ratliff,J.A., Durney,C.H. and Johnson C.C. "Measurement of Radiofrequency Power Absorption in Monkeys, Monkey Phantoms, and Human Phantoms Exposed to 10-50 MHz Fields", Report SAM-TR-76-5, University of Utah.

15. Greene,F.M., "Measurement of RF Power-Absorption in Biological Specimens (10 to 100 MHz)", DHEW (NIOSH) Publication, No. 77-146.

16. Balzano,Q., Garay,O. and Stell,R.F., "Energy Deposition in Simulated Human Operators of 800 MHz Portable Transmitters", IEEE Trans. Veh. Techn., Vol. VT-27, pp. 174-181. Lauderale, Florida.

17. Balzano,Q., Garay,O., and Stell,R.F., "Heating of Biological Tissue in the Induction Field of Portable Radio Transmitters", IEEE Trans. Veh. Techn., Vol. VT-27, pp. 51-56.

18. Bassen,H., Herchenroeder,P., Cheung,A. and Neuder,S., "Evaluation of an Implantable Electric-Field Probe Within Finite Simulated Tissues",Biological Effects of Electromagnetic Waves, URSI Symp., Oct. 11-15, Amhmerst, Mass.

19. Ho,H.S., Edwards,W.P. and Bassen,H., "Measured Internal Electric Field in Phantom Human Heads Exposed to Leakage Radiation from Microwave Ovens", Bicelectromagnetics Symp., June 18-22, Seattle, Wash., 1979.

20. Bassen,H. and Franke, K., "BRH Implantable Probe Evalulation", Draft Report.

21. Bassen,H. and Herman,W., "EM Probe with Fiber Optic Telemetry System", Microwave J., Vol. 20, pp. 35-39.

22. Bassen,H. and Hoss,R.J., "An Optically Linked Telemetry System for Use with Electromagnetic Field Measurement Probes", IEEE Trans. on Electromagnetic Compatibility, Vol. EMC-20, No.4, Nov. 1978.

23. Cowley, A.M. and Sorensen,H.O., "Quantitative Comparison of Solid-State Microwave Detectors", IEEE Trans. Micro. Theory and Techn., Vol. MTT-14, No.12, Dec. 1966, pp. 588-602.

24. Hill, D.A. and Hartsgrove,G.W., "The BRH - NARDA Implantable Miniature Electric Field Probes for Microwave-Bioeffects Studies: An Evaluation and Calibration at 2450 Mhz Using a New Waveguide Technique", Defence Research Establishment Ottawa, Technical Note 00-00, Jan. 1980.

25. Watt, M.D., "UNIIIE", Canada Centre for Remote Sensing, Sept. 1979.

26. Mack, C., "Essentials of Statistics for Scientists and Technologists", Plenum Press, New York, 1967.

27. Kraus, J. D., "Antennas", McGraw-Hill Book Company Inc., 1950.

28. Beyer, W. H., "CRC Standard Mathematical Tables", CRC Press Inc., 1978.

29. Grant,P., "Shielding Barriers Block Electromagnetic Waves", Microwaves, Vol.21, No.6, June 1982.

30. Grant,P., "Emitter / Susceptor Profiles Predict Proper Shielding", Microwaves, Vol.21, No.7, July 1982.

31. Nassif,N.,Silvester,P., "Graphic Representations of Three Component Electromagnetic Vector Fields", M.Eng. Thesis in Electrical Engineering, McGill University, 1982.